

Project Acronym	CORMORAN (ANR 11-INFR-010)
Document Title	D3.2 – Design of Cooperative Location Algorithms (Initial Document)
Contractual Date of Delivery	M21 (09/2013) / M30 (06/2014) [Approved extension]
Actual Date of Delivery	M30 (06/2014)
Editor	CEA
Authors	B. Denis, J. Hamie (CEA), M. Mhedhbi, N. Amiot, B. Uguen (UR1), C. Chaudet (TPT), Arturo Guizar, Claire Goursaud (INSA)
Participants	CEA, UR1, INSA, TPT
Related Task(s)	T3
Related Sub-Task(s)	T3.2
Security	Public
Nature	Technical report
Version Number	1.0
Total Number of Pages	64

Contacts & Correspondence

Benoît Denis (CEA)

- Address: CEA-Leti Minatec, 17 rue des Martyrs, Bât. 51C, p. C455, 38054 GRENOBLE Cedex 9, France
- E-mail: benoit.denis@cea.fr
- Tel: + 33 (0)4 38 78 09 90

TABLE OF CONTENT

TABLE OF CONTENT	3
TABLE OF ACRONYMS	4
ABSTRACT	5
1. INTRODUCTION.....	7
2. REMINDER OF TARGET APPLICATIONS AND RELATED ASSUMPTIONS	8
2.1. Large-Scale Individual Motion Capture (LSIMC).....	8
2.1.1 Relative On-Body Nodes Ranging	8
2.1.2 Relative On-Body Nodes Positioning	9
2.1.3 Absolute On-Body Nodes Positioning	9
2.1. Coordinated Group Navigation (CGN).....	10
2.1.1 Relative Body-to-Body Ranging in a Group	10
2.1.2 Absolute Body Positioning in a Group	10
2.2. Summary of Application Needs.....	12
3. WBAN-BASED SINGLE-LINK RANGING MEASUREMENTS.....	12
3.1. Empirical Modelling of On-Body Ranging Errors Based on IR-UWB TOA Estimation.....	13
3.1.1 Emulated TOA Estimates Based on real Measurements	13
3.1.2 Models and Parameters	15
3.2. Theoretical Modeling of Off-Body and Body-to-Body Ranging errors based on Narrow-Band RSSI Estimations.....	21
3.2.1 Off-Body Links	21
3.2.2 Body-to-Body Links	24
4. WBAN-BASED MOTION CAPTURE ALGORITHMS	25
4.1. Locating On-Body Nodes in a Local Coordinates System.....	25
4.1.1 Cooperative Localization through Constrained Multidimensional Scaling and SVD Decomposition	25
4.1.2 Cooperative Localization through Constrained Distributed Weighted Multidimensional Scaling	33
4.2. Locating On-body Nodes in a Global Coordinates System	46
4.2.1 2-step Algorithm with with Distance Approximation Over Neighborhood Graph	46
5. PRELIMINARY INSIGHTS ON RSSI-BASED COOPERATIVE NAVIGATION IN TYPICAL WBAN INDOOR CONTEXTS	55
6. CONCLUSIONS AND PERSPECTIVES	60
7. REFERENCES.....	62

TABLE OF ACRONYMS

A-B	Aggregate and Broadcast
AWGN	Additive White Gaussian Noise
B-MLE(C)	Biased Maximum Likelihood Location Estimation (Correction)
CAP	Contention Access Period
CDF	Cumulative Density Function
CDWMDS	Constrained Distributed Weighted Multi-Dimensional Scaling
CIR	Channel Impulse Response
CFP	Contention Free Period
CGN	Coordinated Group Navigation
CRLB	Cramer Rao Lower bound
DWMDS	Distributed Weighted Multi-Dimensional Scaling
FAP	First Arrival Path
(G)TS	(Guaranteed) Time Slots
IR-UWB	Impulse Radio – Ultra Wideband
ISM	Industrial Scientific & Medical radio bands
LCS	Local Coordinates System
LMDS	Local Multi Dimensional Scaling
LoS	Line of Sight
LSIMC	Large-Scale Individual Motion Capture
MDS	Multi Dimensional Scaling
MF	Matched Filtering
ML	Maximum Likelihood
MAC	Medium Access Control layer
MoCap	Motion Capture
NB	Narrow Band
NLoS	Non-Line of Sight
PDF	Probability Density Function
PER	Packet Error Rate
PL	Path Loss
RGM	Random Gauss Markov
RMSE	Root Mean Squared Error
RPGM	Reference Point Group Mobility
RSSI	Received Signal Strength Indicator
(RT-)ToF	(Round Trip -) Time Of Flight
Rx	Receiver
SNR	Signal to Noise Ratio
SVD	Eigen/Singular Value Decomposition
TDOA	Time Difference Of Arrival
TDMA	Time Division Multiple Access
ToA	Time of Arrival
TWR	Two Way Ranging
Tx	Transmitter
WBAN	Wireless Body Area Network
xB-MLE	Extended Biased Maximum Likelihood Estimation

ABSTRACT

Wireless Body Area Networks (WBAN), which currently benefit from the emergence of *Ultra Low Power* radio technologies, may be massively disseminated in the near future, as distributed elements of a more global heterogeneous communication architecture. Besides, user-centric and context-aware services have been progressing significantly for the last past years, requiring e.g., that the location information is delivered on the mobile user side, with a limited access to the infrastructure. In the context of wearable networks, new cooperative communication schemes, involving peer-to-peer radio links between mobile nodes or terminals, provide natural interactions at the body scale (i.e. on-body cooperation) and/or between mobile users (i.e. body-to-body cooperation). These cooperative links are not only expected to improve data rates, communication robustness or coverage, but they shall also enable to retrieve relative range measurements, based on the *Round Trip - Time of Flight (RT-ToF)* or *Received Signal Strength Indicator (RSSI)* of transmitted signals. The CORMORAN project aims at investigating such cooperation mechanisms *in* and *between* body area networks, mostly for motion capture/detection and navigation-oriented applications. Determining the adequate cooperation level and modes can help to achieve a precise radiolocation of on-body nodes and/or pedestrians, as well as an optimal management of the communication quality of service at the protocol level, while taking into account the specific characteristics of such wearable networks (e.g., in terms of mobility).

This document, entitled “Design of Cooperative Location Algorithms (Initial Document)” (D3.2), summarizes the work carried out for the first half of the project duration in the frame of sub-tasks 3.2. More specifically, it accounts for the design and preliminary simulation-based validation of WBAN localization algorithms. The latter aim at addressing both *Large Scale Individual Motion Capture (LSIMC)* and *Coordinated Group Navigation (CGN)* application needs identified in sub-task T1.1. First of all, parametric WBAN-specific ranging error models based on real channel measurements are described, characterizing different kinds of cooperative WBAN links (i.e., on-body, off-body and body-to-body) for two key radio low-consumption radio technologies (i.e., *Impulse Radio - Ultra Wideband (IR-UWB)* and *narrow band (NB)* at 2.45GHz). Then estimation algorithms fed by on-body range measurements are proposed so as to retrieve the relative positions of on-body nodes in local body-strapped coordinate systems. These solutions include centralized/synchronous and decentralized/asynchronous variants of *Multi-Dimensional Scaling (MDS)* thus offering gradual levels of complexity and susceptibility to latency. On this occasion, it is shown that introducing a priori heuristics related to the WBAN deployment (e.g., physical body dimensions, existence of fixed-length links under mobility, censoring of peripheral nodes...) can help to significantly reduce estimation errors. One step further, joint single-user navigation and motion capture capabilities are also enabled within a 2-step approach, which combines the previous relative positioning techniques at the body scale with additional transformation operations relying on off-body links with respect to external anchors. It is also shown that missing and/or outlier measurements caused by body shadowing could be mitigated through local graph reconstructions. Finally,

regarding body-to-body cooperation in the context of group navigation, very preliminary results are provided. In particular, the effects on positioning of RSSI-based measurement outliers in typical indoor environments are first characterized, before being mitigated through advanced link selection based on global *Maximum Likelihood* (ML) criteria.

1. INTRODUCTION

This document is related to the subtask 3.2 of the CORMORAN project. This subtask focused on investigating and evaluating localization and tracking algorithms for both motion capture and group navigation applications.

Wireless Body Area Networks (WBAN) can indeed offer intrinsic motion capture/detection capabilities through peer-to-peer ranging and on-body nodes positioning, but also improved navigation means by means of body-to-body and/or off-body links, by relying uniquely on transmitted signals and data packets.

In the recent literature however, most WBAN radio models are still focused on on-body channel characterization from a pure communication-oriented perspective. Besides, in the field of cooperative WBAN localization, most of the algorithmic investigations carried out so far still consider unrealistic synthetic ranging errors based on Time of Arrival (TOA) estimation, hence biasing the evaluation of localization performance. In particular, no ranging-oriented parametric models have been proposed to realistically account for dynamic on-body, off-body and body-to-body links, apart from conventional indoor representations (i.e. regardless of the WBAN context). Thus in this deliverable, we first try to characterize WBAN-based radiolocation metrics and related errors over various kinds of single links (on-body, off-body, body-to-body) out of real WBAN channel measurements.

Applying cooperative localization in the WBAN context also imposes to overcome numerous other challenges. Wearable sensors are indeed subject to drastic constraints in terms of complexity and consumption, but also to very specific mobility patterns. Most algorithms addressing WBAN localization in the recent literature consider only fully centralized resources and synchronous calculi, which may not be totally compliant with real-time constraints under human mobility. Moreover, they often under-exploit the available potential of mesh topologies by sticking with non-cooperative links (i.e. uniquely with respect to fixed anchors). A few solutions also consider a priori parametric models, which may be incompatible with the location-dependent and “unpredictable” mobility patterns experienced by on-body nodes under arbitrary deployment. In this deliverable, we thus describe various algorithmic solutions based on *Muti-Dimensional Scaling* (MDS) to localize on-body wireless nodes relatively to a body-strapped *Local Coordinate System* (LCS), while aiming at better adaptability to local nodes velocities and benefitting from the physical specificities of the cooperative WBAN context. More specifically, one first proposal is to introduce coarse a priori geometric constraints relying e.g., on the prior knowledge of minimal and maximal feasible distances in case of radio connectivity (given the finite dimensions of the full body). In another approach, the locations of mobile on-body nodes are asynchronously estimated using information from their 1-hop neighbors, thus providing better immunity against latency effects under realistic protocol constraints. Fixed-length links (e.g. between the hand’s wrist and the elbow under mobility) can also be incorporated as a priori geometric constraints, hence limiting the number of required on-line measurements, while still benefitting from the mesh cooperative potential. Finally, censoring and/or scheduling of the most demanding nodes when updating estimated

positions mitigate error propagation among the nodes. For all these on-body positioning techniques, the intention is also to verify if and to which extent it is theoretically feasible to address aggressive targeted on-body levels of precision based on currently available on-body radio technologies.

Then, in a heterogeneous WBAN context involving both on-body links and off-body links with respect to external anchors, we put forward a 2-step scheme, where the positions of on-body nodes are preliminary estimated relatively to the body scale, before being expressed into an absolute *Global Coordinates System* (GCS) after a set of transformations. This solution is compared with a second global solution localizing directly the nodes into the GCS using all the available body-to-body and off-body measurements.

Finally, regarding body-to-body cooperation in the context of group navigation, very preliminary results are provided and discussed. RSSI-based measurement outliers are characterized in typical indoor environments are first characterized based on real field experiments. Then various link selection strategies aiming at mitigating the effect of outliers on positioning, including global *Maximum Likelihood* (ML) criteria, are evaluated and compared.

This document is structured as follows: in Section 2, we recall the characteristics and challenges of two main application scenarios, namely CGN and LSIMC. Then in Section 3, we characterize WBAN-based single-link radiolocation models and we briefly discuss related ranging errors for further evaluation. In Section 4 and 5, we describe and evaluate positioning and tracking algorithms for LSIMC and CGN, respectively. Finally, Section 6 discloses perspectives for the next and final version of this deliverable (D3.5).

2. REMINDER OF TARGET APPLICATIONS AND RELATED ASSUMPTIONS

In this section, we first recall the needs, definitions and challenges of the main applicative scenarios of interest, already specified in details in D1.1 [CORMORAN_D1.1].

2.1. LARGE-SCALE INDIVIDUAL MOTION CAPTURE (LSIMC)

2.1.1 RELATIVE ON-BODY NODES RANGING

In this first sub-scenario, one considers a set of mobile wireless devices placed on one single body (under arbitrary deployment), with unknown positions. The objective is then uniquely to estimate the relative Euclidean distances separating those nodes. Accordingly, at each time stamp, one can retrieve a relative body topology, independently of the way the underlying nodes coordinates could be expressed or referenced (i.e. whatever their reference coordinate system). Only the relative range information is of interest. This mode shall remain marginal in our context, since most of the targeted use cases would require that the nodes coordinates are explicitly expressed into a local (i.e. body-strapped) system or into a global absolute system (likely external to the body), as seen in the two following paragraphs.

2.1.2 RELATIVE ON-BODY NODES POSITIONING

In this second sub-scenario, we consider a set of wireless devices placed on a body, which can be classified into two categories. Simple mobile nodes with unknown positions (still under arbitrary deployment) must be located relatively to reference anchor nodes, which are attached onto the body at known and reproducible positions, independently of the body attitude and/or direction (e.g. on the chest or on the back). A set of such anchors can thus define a Cartesian *Local Coordinates System* (LCS) under mobility, which remains time-invariant (i.e. as expressed in the LCS) under body mobility. The estimated coordinates of the mobile nodes are then expressed into this LCS. This functionality is also occasionally depicted as “Nodes positioning at the body scale”.

2.1.3 ABSOLUTE ON-BODY NODES POSITIONING

This last sub-scenario is the same as the previous one, but the coordinates system used to express the estimated on-body mobile nodes locations is no more body-strapped but external to the body.

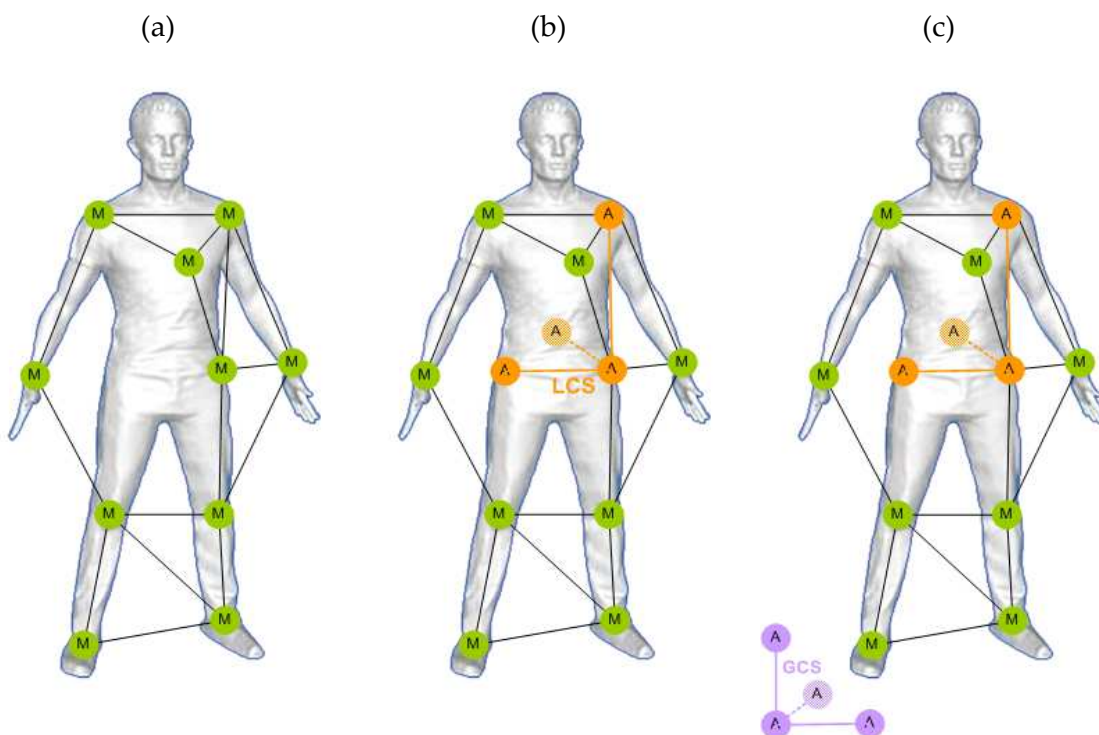


Figure 2.1: Examples of relative on-body nodes ranging (a), relative on-body nodes positioning (b) and absolute on-body nodes positioning (c) configurations for large-scale single-user motion capture applications.

In this framework, one may thus consider as anchor nodes, some fixed elements of infrastructure (e.g. beacons/landmarks, base stations, access points or gateways) disseminated at fixed known locations in the environment. Accordingly, the coordinates of the nodes placed on the body chest or back, which used to be time-invariant in their LCS, shall now vary in a

Global Coordinates System (GCS) under pedestrian mobility. They directly depend on the body attitude, as well as on the motion direction and/or speed. By default, this sub-scenario, which makes sense since we claim a “large-scale” nomadic service in comparison with video systems that operate in more restricted geographical areas (due to the presence of relatively dense and heavy pieces of infrastructure), will be the preferred motion capture sub-scenario in the following. It may also be viewed as a combination of relative motion capture (i.e. at the body scale) and classical single-user navigation capabilities. Finally, note that defining the on-body nodes locations into a LCS may be still required here, as an intermediary step of the calculations.

2.1. COORDINATED GROUP NAVIGATION (CGN)

2.1.1 RELATIVE BODY-TO-BODY RANGING IN A GROUP

In this first navigation sub-scenario, people wearing several on-body wireless sensors and forming a group of mobile users must localize them-selves with respect to other mates in the very group. The inter-body range information is required, that is to say, only the relative group topology, independently of the actual locations (and orientations) in the room or in a building. Accordingly, no external anchor nodes would be required in this embodiment.

2.1.2 ABSOLUTE BODY POSITIONING IN A GROUP

In a second preferred sub-scenario, which is intended in a more classical pedestrian navigation sense, one must retrieve the absolute coordinates of several users belonging to the same mobile group, with respect to an external GCS. This shall imply the use of fixed and known elements of infrastructure around, like previously within large-scale motion capture applications based on absolute on-body nodes positioning. In comparison with other State of the Art navigation solutions, the presence of multiple wearable on-body nodes (i.e. in the WBAN context) is expected to enhance navigation performance by providing spatial diversity and measurements redundancy (i.e. over off-body links with respect to the infrastructure and/or over inter-WBAN/body-to-body links with respect to other mobile neighbours), and possibly, further cooperative on-body information exchanges (i.e. through intra-WBAN links).

Without loss of generality, note that navigation-oriented scenarios will aim at retrieving mostly the “macroscopic” position of the body, but note the on-body-nodes in details... Hence, a reference point on the body shall be chosen to account for this average position (e.g. the geometric center of the body torso or the barycenter of all the on-body nodes).

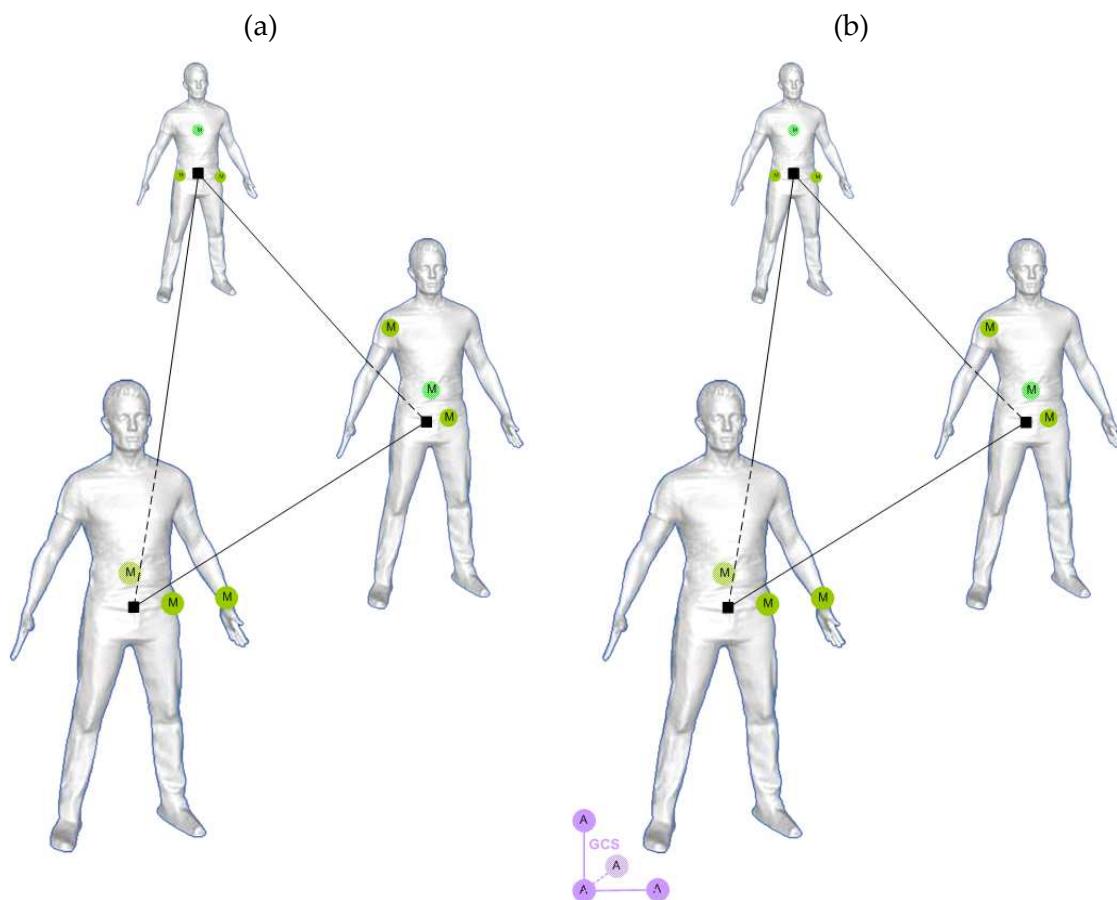


Figure 2.2: Examples of relative body-to-body ranging (a) and absolute body positioning (b) configurations for coordinated group navigation applications.

2.2. SUMMARY OF APPLICATION NEEDS

Table 2-1 summarizes the main needs for the two identified classes of application.

	Large-Scale Individual Motion Capture		Coordinated Group Navigation
	Low Precision	High Precision	
On-Body Nodes Location Precision (Relative)	$\epsilon_{90} < 25$ cm (worst case CDF @ 90%) $\epsilon_{50} \approx 5$ cm (median CDF @ 50%)	$\epsilon_{90} < 5$ cm (worst case CDF @ 90%) $\epsilon_{50} \approx 1$ cm (median CDF @ 50%)	N/A
Average Body Location Precision (Absolute)	$\epsilon_{90} < 1$ m (worst case CDF @ 90%) $\epsilon_{50} \approx 0.3$ m (median CDF @ 50%)		
Nodes Location Refreshment Rate	100 ms	10 ms	1s
Maximum Speed	{5, 15} km.h ⁻¹		
Anchors Density	< 0.05 anchors / m ²		< 0.01 anchors / m ²
Nb Persons per Group	N/A		{5, 10}
Maximum Inter-Body Distances	N/A		{1, 5, 10, 50}
Nb of On-Body Nodes	{5, 10, 20}		{2, 5}
Rank of Preferred On-Body Nodes Location	An-He-Wr-To-Hi-Lg-Ba-Sh-Kn-Bd		Sh-To-Ba-Hi-Wr
Environment	{Outdoor, Indoor}		Indoor
Place for Final Location Info	{Server, User}		User
Pre-Calibration (Deployment Convention to be Respected)	{None, Precise Deployment Pattern}		{None, Rough Deployment Pattern}

Table 2-1 : Summary of application needs in both large-scale individual motion capture (Within low precision and very high precision modes) and group navigation applications¹.

In D1.1 [CORMORAN_D1.1], possible cooperative WBAN deployment options are also reported, including heterogeneous configurations.

3. WBAN-BASED SINGLE-LINK RANGING MEASUREMENTS

In this section, we analyse possible models and parameters characterizing ranging errors based on the two main foreseen WBAN radio technologies, namely *Impulse Radio – Ultra Wideband* (IR-UWB) for on-body, body-to-body and off-body links on the one hand, and *Narrow-Band* (NB) at 2.4 GHz for body-to-body and off-body links on the other hand. In particular, we describe an original on-body error model, based on IR-UWB ToA estimation and exploiting real dynamic channel measurements over two representative on-body links

¹ An : Ankles ; He : Head ; Wr : Wrist ; To: Torso; Hi: Hips; Lg: Legs; Ba: Back; Sh: Shoulders; Kn: Knees; Bd: Bends

and frequency bands [HDER_ACM13], [HDER_BOD12]. Then we discuss theoretical ranging error models over off-body and body-to-body links, respectively for NB RSSI estimation and IR-UWB TOA estimation in the presence of multipath. The latter error characterizations are fed with realistic empirical parameters issued from different WBAN channel measurement campaigns. They will be partly used for evaluation purposes in further studies regarding WBAN-based positioning and tracking algorithms, as seen in the following sections 4 and 5.

3.1. EMPIRICAL MODELLING OF ON-BODY RANGING ERRORS BASED ON IR-UWB TOA ESTIMATION

We present here a first model accounting for dynamic intra-WBAN ranging errors based on IR-UWB ToA estimation in the [3.1, 5.1]GHz and [3.75, 4.25]GHz frequency bands. The latter is compliant with one mandatory band imposed by the IEEE 802.15.6 standardization group. Relying on time-variant on-body channel measurements, we draw our ranging error model as a mixture-based conditional probability density function, taking into account i) dynamic *Signal to Noise Ratio* (SNR) variations and ii) channel obstruction conditions, i.e. *Line Of Sight* (LOS) vs. *Non Line Of Sight* (NLOS), experienced over representative on-body links while walking. The evolution of density parameters is thus characterized as a function of these channel and SNR configurations, illustrating e.g. missed/false path detection effects under low SNR.

3.1.1 EMULATED TOA ESTIMATES BASED ON REAL MEASUREMENTS

- *Considered TOA Estimators*

Out of received noisy multipath signal, the TOA estimation step aims at determining the arrival time of the direct multipath component that would be ideally received in a free space propagation case. The quality of TOA estimation depends on multiple factors such as the emitted pulse energy (and hence, the received pulse energy) in comparison with the noise floor, multipath fading effects (and hence, the occupied bandwidth), or signal obstructions. It is thus possible to generate false alarms due to early noisy realizations or to miss the direct path due to poor SNR conditions and/or severe NLOS blockages. The latter tend to increase the apparent length of the direct path or they can even cause its absence, leading to overestimated ranges.

In this TOA estimation context, *Matched Filtering* (MF), which is one of the most basic reception techniques, is generally characterized by relatively low complexity and low consumption, as claimed in [HS_PhD_10], [SENB_10]. Since WBAN nodes are strongly constrained with this respect, MF is also a rather convenient solution in our context. ToA estimates are thus obtained through strongest peak detection, by looking for the time shift that maximizes the cross-correlation function between the received signal and a local template, which theoretically corresponds to the unitary transmitted waveform.

On the other hand, the *First Arrival Path* (FAP) detection scheme simply consists in preliminarily estimating the *Channel Impulse Response* (CIR) out of the received signal, and

associating the first estimated multipath component (i.e. among all the resolved paths) with the estimated distance (or equivalently Time of Flight) between the transmitter and the receiver. Unfortunately, in NLOS conditions, this FAP may suffer from significant power attenuation that makes it subject to missed/late detections or early false alarms, thus conducting to large estimation errors and, more generally speaking, to a higher dispersion of the measurements.

- *Modeling Methodology*

We consider the dynamic radio channels associated with the Hip-Chest and Hip-Wrist links (as representative WBAN links with different behaviour) from a past measurement campaign described in [EO_09], where the total recording time was 4 sec and consecutive temporal channel responses were collected every 20 ms in the band [3.1, 5.1]GHz. The measurements were performed under moderate human walk mobility in a typical indoor environment, resulting in a set of 200 time-stamped channel responses. For each response, multipath components were extracted using a CLEAN-like high resolution-algorithm [DK_07] in the bands [3.1, 5.1]GHz and [3.75, 4.25]GHz.

Then in order to synthesize a realistic received signal out of the extracted CIRs, as a function of a given initial SNR level and occupying a given bandwidth, a reference template waveform has been applied. Gaussian-windowed sine waves have thus been generated in the [3.1, 5.1]GHz and [3.75, 4.25]GHz bands, the latter being in compliance with one mandatory band specified by the IEEE 802.15.6 band-plan. Those templates are subsequently convolved with the CIRs previously extracted out of real measurements, and an AWGN process with a two-sided power spectral density N_0 (i.e. $N_0 = -154$ dBm/Hz) is filtered into the considered signal band and the convolved useful signal is scaled in energy so as to respect the priori SNR level at an arbitrary time stamp t_0 (here chosen as the time offering the highest channel gain).

At each observation time-stamp, ToA estimates are thus issued from each synthesized noisy received signal, using the two kinds of estimators described in the previous section, namely the strongest path detection based on matched filtering and the first path detection. In our case, the search temporal window has a time length of 5 ns like in [DRBT_07], [SENB_10]. This duration is sufficient in WBAN applications to observe an arrival time corresponding to the maximum distance between two synchronized nodes placed on the same body. Thus we discard too large excess delays. The second FAP detection relies on the results produced by the CLEAN-like channel estimation approach [DK_07].

The first Hip-Chest link is always assumed in LoS conditions, whereas the Hip-Wrist link varies dynamically, leading periodically and alternatively to LoS and NLoS conditions. In order to classify the obstruction conditions, the retained method is based on the power transfer function derived from measurements. During the initial communication-oriented measurement campaign reported in [EO_09], the real distance between nodes was not collected, since measurements were not carried out for localization purposes. However, in first approximation, one can try to extract this distance out of the measured ToA in time-stamp

regions when the LOS conditions are clearly identified and with very high SNR for the synthetic received signals in the largest bandwidth [3.1, 5.1]GHz. Practically, the first Hip-Chest link is considered as fixed and the reference distance extraction is directly realized by averaging all the ToA measurements issued from MF estimation over the walk cycle to reduce ToA estimation errors appeared in presence of overlapping components. Nevertheless, for the second Hip-Wrist link, a smoothing process was performed in a sliding window whose length corresponds to 20 consecutive time-stamp samples (e.g. within $20 \times 20\text{ms} = 400\text{ms}$). The true distance was subsequently interpolated over identified NLoS portions of time, assuming continuity of the true distance at LoS/NLoS boundaries but discontinuity for the smoothed version of the measured distance (obtained with the sliding window). Figure 3.1 show examples of obtained traces as a function of time-stamp at high SNR.

A more detailed and complete description of the previous methodology is available in [HDER_ACM13], including multipath extraction out of real channel measurements, SNR-dependent and bandwidth-dependent synthetic multipath re-generation with power scaling, application of ToA estimators and averaging/interpolations.

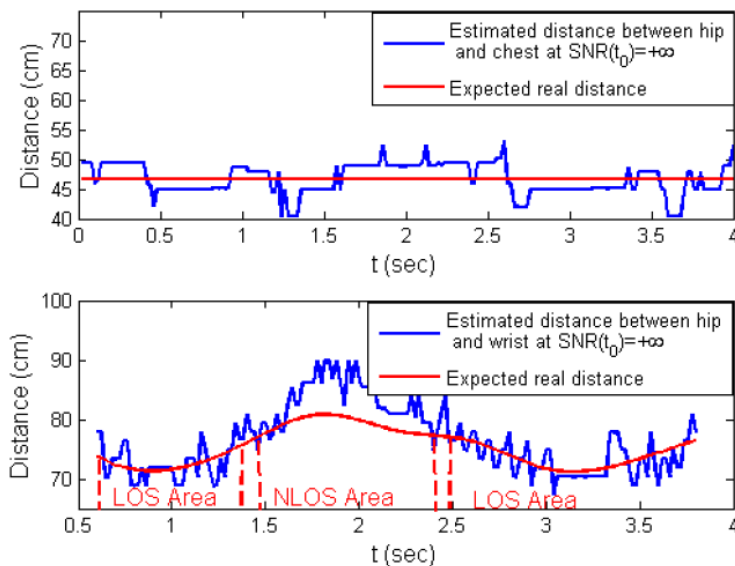


Figure 3.1: Equivalent inter-node distance retrieved out of correlation-based ToA estimation without noise (blue) and fitted reference distance after averaging with a sliding window and splines interpolation over the detected NLoS time stamp region (red), for both Hip-Chest (top) and Hip-Wrist links (bottom).

3.1.2 MODELS AND PARAMETERS

We now aim at statistically characterizing the obtained ToA-based ranging error observations in the [3.1, 5.1]GHz and [3.75, 4.25]GHz frequency bands, for the two kinds of on-body radio links. As previously mentioned, these models are conditioned on the channel obstruction status and on the reference SNR(t_0). While running simulations, for each SNR(t_0) value, 100 independent noise process realizations are drawn for the walk cycle duration. Over these

realizations, for each frequency band, up to 20000 range measurements are then collected in LoS conditions for the Hip-Chest link, whereas 8600 and 3800 measurements are generated for the Hip-Wrist link, respectively in LoS and NLoS conditions.

- *LOS Model*

For the strongest path detection strategy based on matched filtering, conditioned on the LoS case, it appears that the step-wise empirical *Cumulative Density Function* (CDF) of emulated range measurements enjoys a rather satisfactory fit (in a least squares sense) to the CDF of a Gaussian random variable, whose standard deviation is on the order of the time base sampling period. Figure 3.2 shows examples for both simulation-based and model-based (with fitted parameters) LoS CDFs with $SNR(t_0) = 5\text{dB}$ in the band $[3.1, 5.1]\text{GHz}$.

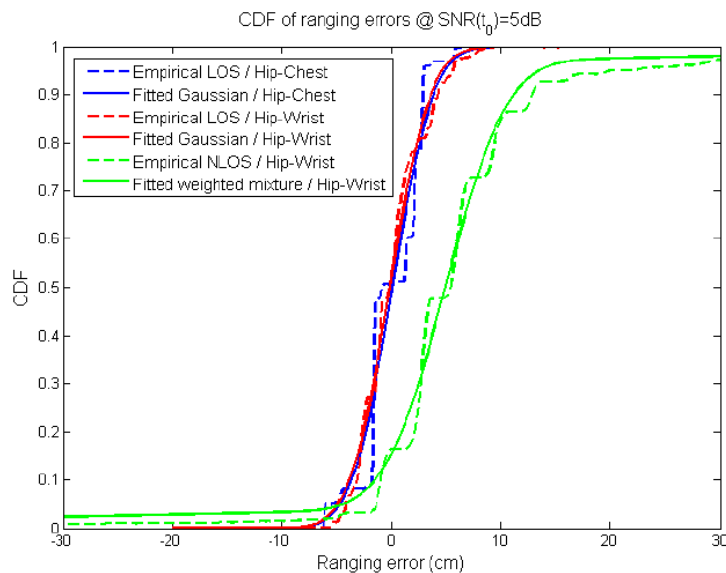


Figure 3.2: Empirical and model-based CDFs of ranging errors in both LoS and NLoS conditions with a matched filter (strongest path detection), with $SNR(t_0) = 5\text{dB}$ in the band $[3.1, 5.1]\text{GHz}$.

Figure 3.3 and Figure 3.4 show respectively the variations of the mean and standard deviation of the corresponding Gaussian LoS model for both links and both bands, as a function of $SNR(t_0)$. As seen in Figure 3.3, the mean varies around zero, with very low relative values (in comparison with the nominal expected true range value), and hence, it can be considered as null in first approximation over the explored range of $SNR(t_0)$ values. Figure 3.4 shows that the behaviour of the standard deviation is asymptotically constant when $SNR(t_0)$ reaches a value of 10dB. At high SNRs, the strongest path detected through cross-correlation indeed coincides systematically with the direct path. The asymptotic error at high SNR thus depends mostly on the occupied bandwidth and centre frequency. To summarize, considering the tested Hip-Chest and Hip-Wrist links, the distribution of the ranging error through correlation-based TOA estimation in LoS conditions in the $[3.1, 5.1]\text{GHz}$ and $[3.75, 4.25]\text{GHz}$ bands can be simply modelled as a centred Gaussian distribution, with a standard deviation

depending on the bandwidth B and $SNR(t_0)$ (See the legend of Figure 3.4 for detailed model parameters).

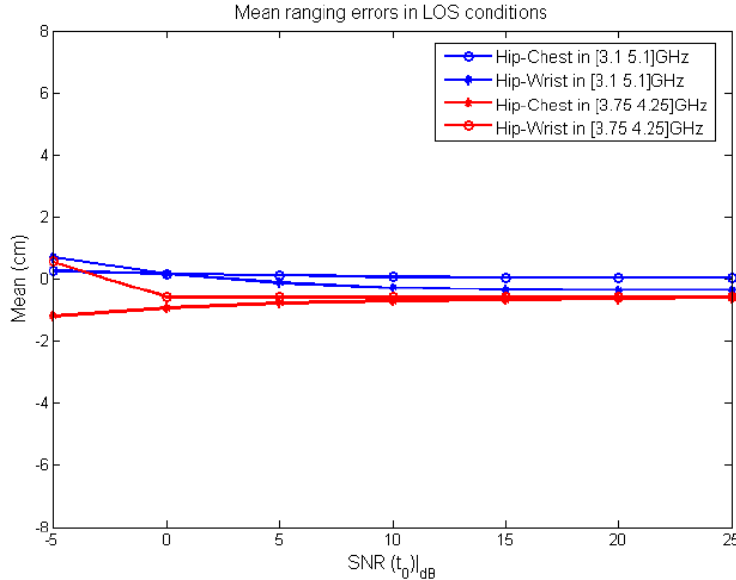


Figure 3.3: Mean of ranging errors in LoS conditions with a matched filter (strongest path detection), as a function of $SNR(t_0)$.

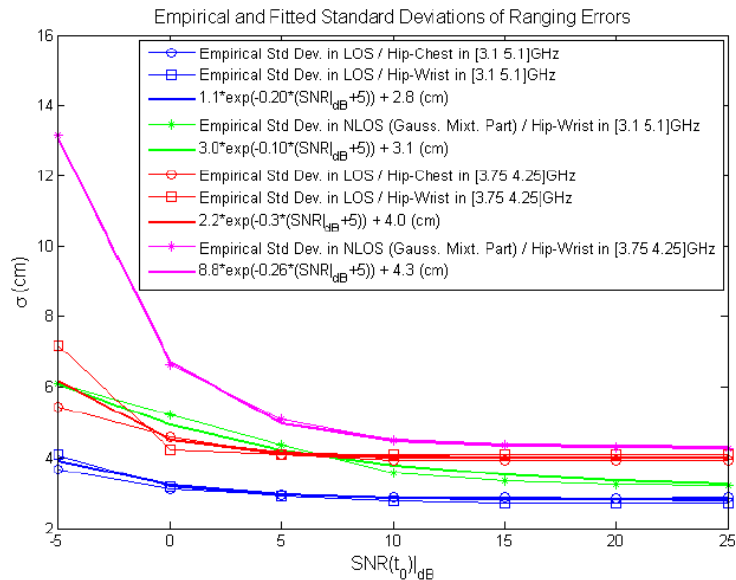


Figure 3.4 : Standard deviations of ranging errors in LoS and NLoS conditions with a matched filter (i.e. strongest path detection), as a function of $SNR(t_0)$.

As for ToA estimation through FAP detection, we observed that the resulting *Probability Density Function* (PDF) could be better represented by a mixture involving Gaussian and Uniform components. The Uniform distribution is weighted by the false alarm probability PF , which represents the probability to detect a wrong peak instead of the true FAP. PF is thus strongly affected by the threshold chosen within the FAP detection scheme (e.g. a smaller threshold obviously leads to higher PF), and hence, by the stopping rule in the underlying

high-resolution channel estimation algorithm. Figure 3.5 shows the variation of PF as a function of SNR(t_0) for both links in the [3.1, 5.1]GHz frequency band. At high SNR(t_0), the behaviour appears to be almost Gaussian and PF is approximately null. Figure 3.6 and Figure 3.7 show respectively the variations of the mean and standard deviation of the corresponding Gaussian distribution component, for both links in the band [3.1, 5.1]GHz. These variations are compliant with the variations observed in the matched filter case in case of strongest path detection. This result shows that, in general LoS conditions, the FAP is rather in line with correlation-based ToA estimation. Thus one could reasonably apply systematic strongest path detection for lower complexity in such favourable conditions.

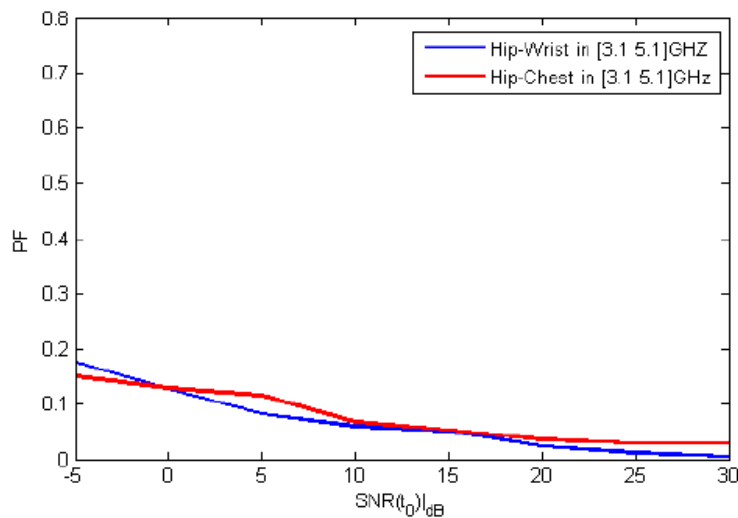


Figure 3.5 : Variation of the false alarm probability for FAP ToA estimation (i.e. first path detection), using a threshold of 10 dB below the global absolute maximum of the estimated CIR, in LoS conditions, in the band [3.1, 5.1]GHz, as a function of SNR(t_0).

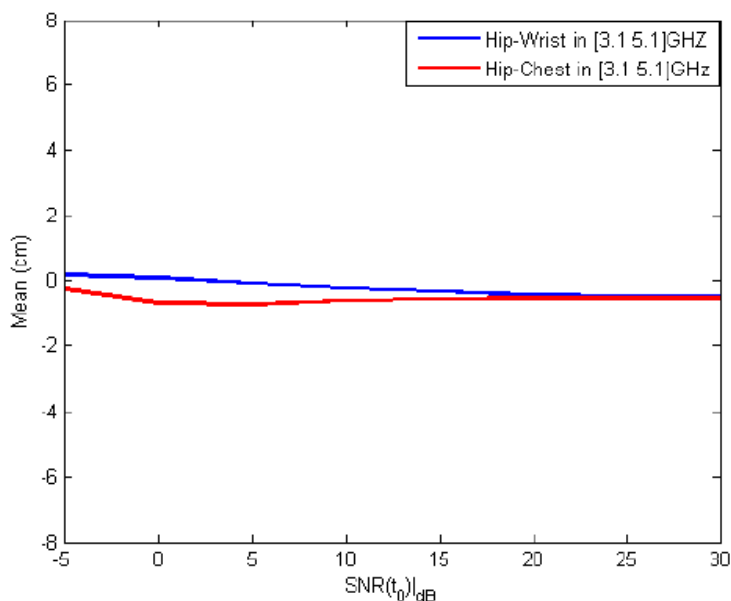


Figure 3.6 : Mean of ranging errors for FAP ToA estimation (i.e. first path detection), in LoS conditions in the band [3.1, 5.1]GHz, as a function of SNR(t_0).

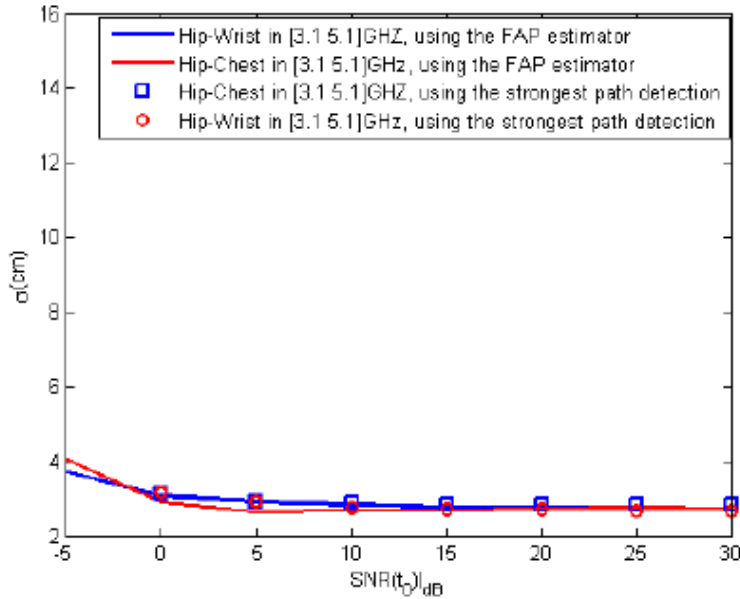


Figure 3.7 : Comparison between the standard deviations of ToA-based ranging errors using a FAP ToA estimator (i.e. first path detection using a threshold of 10 dB below the global absolute maximum of the estimated CIR) and a strongest correlation peak ToA estimator, in LoS conditions, in the band [3.1, 5.1]GHz, as a function of SNR(t₀).

- *NLOS Model*

In NLoS conditions (i.e. under body shadowing), the best fit has been obtained to a mixture-based model involving Gaussian and Uniform components. Figure 3.2 shows examples of both the empirical and model-based NLoS CDFs at SNR(t₀) = 5dB, in the [3.1, 5.1]GHz band. The corresponding conditional *Probability Density Function* (PDF) is then expressed as follows:

$$p(e) = \psi U(T_w) + (1 - \psi)G(\mu, \sigma^2)$$

where $p(e)$ is the PDF of the random ranging error e in NLoS conditions, $U(T_w)$ is a uniform distribution, whose temporal support T_w depends on the receiver observation window while performing ToA estimation through cross-correlation. Again, this window is chosen to enable detection within any intra-WBAN link after synchronization (e.g., considering typically a worst case distance of 1.5m, or equivalently 5 ns), ψ is the weight of the uniform distribution, and $G(\mu, \sigma^2)$ is a Gaussian distribution with a mean μ and a variance σ^2 . The variation of those parameters in both bands of interest, as a function of SNR(t₀) is represented in Figure 3.4, Figure 3.8 and Figure 3.9. As shown on Figure 3.9, at low SNR(t₀), the contribution of the uniform distribution component is high. This effect accounts for the distribution of the so-called apparent path arrival determined through cross-correlation over the entire observation window (e.g. between 0 and 5ns), when the noise level is so high that it can cause frequent missed detections or false alarms. The uniform weight in the mixture then directly reflects the probability of having either a false alarm or a missed detection. However, at higher SNR(t₀), the behaviour is almost Gaussian, where the ranging error is centred around a positive mean,

which can be interpreted as a positive bias caused by the obstruction of the direct path (and hence, its apparent length extension).

As shown in Figure 3.4, at high SNR(t_0) (i.e. larger than 10dB), in each operating band, the behaviour of the error standard deviation in LoS is similar to that of the Gaussian part of the mixture-based NLoS model, as the uniform weight is becoming quasi-null. Similar standard deviations means that the path detection performances are thus equivalently good in terms of dispersion in LoS and NLoS conditions, given the observed strongest path. However, it is worth keeping in mind that the apparent time of flight of the first observable path in NLoS cases is shifted independently of the path power, hence leading to a non-neglected ranging bias (i.e. besides random noise terms). The fact that the NLoS bias is approximately constant over SNR(t_0) for a given band is also in line with the previous remarks. This very bias value, which seems to depend mostly on the occupied band, is rather hard to predict (as a deterministic parameter) and characterize further in practice. Hence, we recommend in our final ranging error model to assume this bias as a Uniformly distributed random variable, drawn once for all within a plausible range of a few tens of cm (i.e. with a realization that is valuable approximately constant over all the NLoS portions of one given walk cycle).

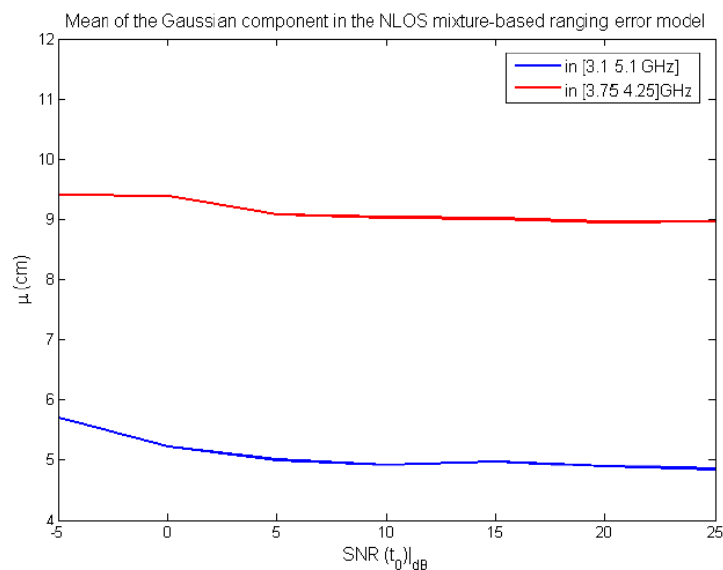


Figure 3.8: Mean value associated with the Gaussian part of the ranging error mixture-based model in NLoS conditions, as a function of SNR(t_0).

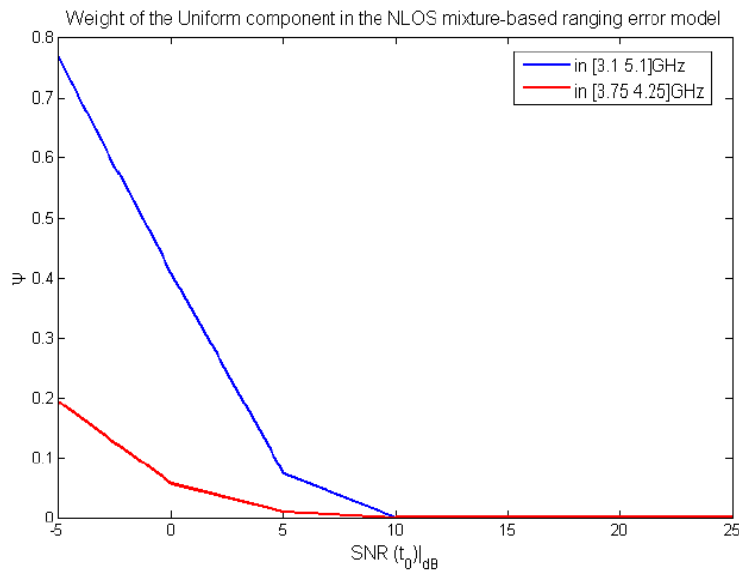


Figure 3.9: Weight of the Uniform part of the mixture-based ranging error model in NLoS conditions, as a function of SNR(t_0).

More complete tables with model parameters as a function of the bandwidth and SNR are available in [HamiePhD_13] for simulation purposes (i.e., to generate realistic traces of on-body ToA-based ranging measurements under mobility), along with a discussion about the possibility to generalize the model to other on-body links.

3.2. THEORETICAL MODELING OF OFF-BODY AND BODY-TO-BODY RANGING ERRORS BASED ON NARROW-BAND RSSI ESTIMATIONS

In *Narrow-Band* (NB) RSSI-based ranging approaches, the best standard deviation is proportional to the ratio between the shadowing standard deviation and the path loss exponent. Intuitively, a high ratio indeed implies that the dependency of the decrease of the average received power as a function of the log-distance separating the transmitter and the receiver is no longer significant nor dominating in comparison with the shadowing dispersion (i.e. around this mean power). This would make the interpretation of RSSI readings more challenging from ranging perspective. Applying a *Cramer Rao Lower bound* (CRLB) expression for discussions, using recent experimental channel model parameters (i.e. path loss and shadowing parameters) obtained over off-body and body-to-body links, which have been specified in the *Industrial Scientific & Medical* (ISM) band at 2.45 GHz.

3.2.1 OFF-BODY LINKS

Off-body links involve two kinds of wireless devices. The first one is placed on the body and the second one belongs to the surrounding infrastructure, most likely set as an anchor in our localization problem. These links are thus likely asymmetric since on-body devices are subject to more drastic constraints in terms of transmission ranges and consumption, contrarily to elements of infrastructure.

Inspired from the off-body channel model in [RE_12], which has been specified at 2.45 GHz according to the IEEE 802.15.4 standard, the used RSSI model can be simplified by eliminating the fast fading components (i.e. considering that one would average over a sufficient number of consecutive RSSI readings for each pair-wise link in a real system). The RSSI model is thus similar to conventional models, all except but the body shadowing, which mainly (and somehow deterministically) depends on the body orientation with respect to the external node. In a few scenarios however, frank LoS and NLoS configurations have been tested, with the subject body respectively facing or giving his back to the external node. Table 3.1 summarizes the corresponding parameters in an indoor environment for WBAN planar monopole antennas over two different specific links, namely with on-body nodes positioned on the heart or on the left hip of the subject body.

One first remark is that the reference path loss is no longer unique but it rather strongly and adversely depends on both the on-body node's location and the antenna kind (depending on the antenna pattern). This is one more challenging point for off-body RSSI-based ranging. In other words, if this disparity cannot be treated a priori as a nuisance and additional source of randomness (e.g. as part of an extended "shadowing" modeling), this practically implies that the reference path loss (again, assumed known by RSSI-based ranging algorithms) would have to be preliminarily calibrated out, not only once for all with one single reference on-body node in a given environment, but for each of the possibly occupied on-body locations, what is particularly time consuming. Another remark is that the path loss exponent < 1 is very low in frank NLoS cases, whereas the measured power dispersion is large (on the order of 10 to 12 dB) showing that the randomness of the multipath contributions globally removes the distance dependency. But in practical cases, LoS/NLoS configurations cannot be classified so easily into binary cases over off-body (or even over body-to-body) links but there is a continuum of body shadowing configurations, as a function of the subject orientation, depending if the body partially or totally obstructs the propagation of direct radio waves. In [RE_12] for instance, it has been shown that the power fluctuations observed over a full body rotation of 360° could be as large as 25 dB overall for a given on-body node's location (e.g. the hearth) and a given antenna (e.g. the planar monopole), regardless of the actual distance from the external node. In other words, from the RSSI-based ranging perspective, if the body shadowing term is still modeled as a Gaussian random variable after averaging over all the possible body orientations, with non-conditional statistics (i.e. regardless of LoS/NLoS), one could assume a standard deviation on the order of 4 dB or more. For illustration purposes, Table 3.2 reports the mean body shadowing values observed as a function of the body-to-external relative angle, over off-body NB links at 2.45 GHz for a planar monopole antenna and an on-body device placed on the heart. Considering similar results for the on-body device placed on the hip and for the same antenna, if one still wants to differentiate between LoS and NLoS cases, after partitioning respectively the results from [RE_12] into the LoS and NLoS angular domains and considering the respective shadowing dispersions over each domain, it is thus reasonable to state that the standard deviation of the body shadowing term is around 1.5 to 2 dB in LoS and 3 dB in NLoS. Note that this representation would artificially lead to extra biases on the received power, accounting for the assumed centered regime around the mean of the body

shadowing, which can be calibrated out (and likely incorporated in the original reference path loss parameter, conditioned on the LoS/NLoS obstruction configuration). As such, these extra mean terms would however not play a role in the CRLB characterizing the RSSI-based ranging performance.

To extend the discussion, additional illustrations for the best achievable RSSI-based ranging error standard deviation under LoS conditions, for an on-body device placed on the heart or on the hip indifferently, are available in [HamiePhD_13]. This standard deviation seems to be rather penalizing, even for the most favorable shadowing standard deviations on the order of 1.5 dB, as extracted from [RE_12], but mostly at large transmission ranges in comparison with the actual distance (e.g., ranging deviation of more than 5 m at 50 m). Even more harmful effects due to NLoS conditions on off-body ranging performance are observable at shorter ranges, especially for typical shadowing standard deviations on the order of 3 dB, as extracted from [RE_12] (e.g., ranging deviation of more than 10 m at 30 m).

As shown in Table 3.1, the path loss exponent appears to be much smaller in NLoS than LoS conditions, meaning that the deterministic dependency of the received power on the true distance is no more significant but start being dominated by shadowing randomness (i.e. all the more dominated since the standard deviation is large). Accordingly, it is hard to interpret the received power for ranging purposes and the corresponding single-link errors are expected to be even larger. These results seem to confirm that RSSI is not a meaningful location-dependent metric in NLoS cases due to hard body shadowing. Hence, RSSI shall be mainly recommended as an indirect source of ranging information over NLoS off-body links and/or NLoS body shadowing mitigation techniques must be figured out, as seen e.g., in the following section 5.

	LOS		NLOS	
	n_p	PL_0	n_p	PL_0
Rx heart	2	-38.92 dB	0.4	-62.62 dB
Rx left hip	2	-51.94 dB	0.1	-68.78 dB

Table 3.1: Path loss model parameters over indoor off-body NB links at 2.45 GHz, according to [RE_12].

Relative Angle (°)	0	45	90	135	180	225	270	315
Body Shad. (dB)	0	-2.77	-9.5	-27.34	-24.99	-17.03	-22.77	-12.4

Table 3.2: Mean body shadowing as a function of the body-to-external relative angle, over off-body NB links at 2.45 GHz for a planar monopole antenna and an on-body device placed on the heart, according to [RE_12].

3.2.2 BODY-TO-BODY LINKS

In [REV_12], the authors have also proposed a new RSSI model for body-to-body links. Table 3.3 summarizes the path loss parameters for a planar monopole antenna over two different specific body-to-body links in LoS and NLoS configurations, under the same relative angular definition as for off-body links (i.e. with one body experiencing a relative angle of 0° for LoS and 180° for NLoS, with respect to the second body).

In first approximation, [REV_12] has also considered the body shadowing as a zero-mean Gaussian variable, characterizing the corresponding standard deviation at around 6 dB over different body-to-body links and regardless of the LoS/NLoS regime. However, the behavior of the body shadowing clearly looks bi-modal instead in our own interpretation and understanding. Each of the modes actually corresponds either to the LoS case or to the NLoS case, respectively centered around +5 or -5 dB, and with a standard deviation on the order of that previously extracted for off-body links, that is to say, around 2 dB in LoS and slightly larger than 3 dB in NLoS. In other words, and in first approximation, the same kind of error regimes could be reasonably applied for both off-body and body-to-body links. One could even observe worse cumulative effects in case of deep NLoS caused by double-body shadowing (the two bodies showing mutually their back).

Similarly to the off-body discussion, it is possible to carry out a parametric CRLB-based study of the best ranging standard deviation achievable over body-to-body links, still assuming that the body shadowing is a Gaussian variable. In [HamiePhD13], for the two previous body-to-body links under LoS and NLoS conditions, the same observations and conclusions as in the off-body case can thus be drawn for off-body links, preventing from exploiting RSSI readings for direct ranging purposes over single links in NLoS configurations due to body shadowing, unless mitigation techniques are employed.

	LOS		NLOS	
	n_p	PL_0	n_p	PL_0
Rx Heart	1.14	-54.02 dB	0.67	-70.77 dB
Rx Right Hip	3.33	-37.88 dB	1.15	-66.63 dB

Table 3.3: Path loss parameters over indoor body-to-body N-B links at 2.45 GHz for a Tx on the Right Hip (first carrying body) and a Rx on the Heart or the Right Hip (second carrying body), according to [REV_12].

Resulting realistic RSSI-based ranging models specific to the WBAN context will be considered in the following sections as well.

4. WBAN-BASED MOTION CAPTURE ALGORITHMS

4.1. LOCATING ON-BODY NODES IN A LOCAL COORDINATES SYSTEM

4.1.1 COOPERATIVE LOCALIZATION THROUGH CONSTRAINED MULTIDIMENSIONAL SCALING AND SVD DECOMPOSITION

As a very first step of our investigations, this subsection introduces a nominal centralized and synchronous solution (i.e., all the on-body nodes positions are estimated simultaneously) estimating the human motion based on a classical *Multi-Dimensional Scaling* (MDS). Different enhancements are also proposed to take in to account the WBAN specificities.

- *Basic LMDS*

Local MDS (LMDS) is a well-known localization technique enabling to retrieve some sensors' locations, knowing only the relative distance between each pair of points.

Conceptually, LMDS is divided in three stages:

- 1- Distance estimation: collects and combines distance measurements into distance matrix
- 2- Pre-placement: produces a set of points according to the distance matrix
- 3- Restoration of the coordinate system: reestablish the coordinate system by changing the basis of the set of points produced in the previous stage.

Consider a network comprising n sensors (e.g., in our case 41), with m -D positions X_i , $i = 1..n$, and $\mathbf{X} = [X_1, X_2, \dots, X_n]^T$ a $n \times m$ matrix collecting these positions (e.g., with $m=3$ in our application context).

Let now $\mathbf{D} = [d_{ij}]$ be the $n \times n$ matrix of pair-wise distance measurements, where d_{ij} is the distance between on-body nodes X_i and X_j . The general goal of LMDS is to find an assignment to \mathbf{X} that minimizes a cost function defined as:

$$F(\mathbf{X}) = \sqrt{\frac{\sum_{i=1}^n \sum_{j=1}^{i-1} (d_{ij} - \delta_{ij})^2}{\sum_{i=1}^n \sum_{j=1}^{i-1} \delta_{ij}^2}}$$

where δ_{ij} is the real distance between X_i and X_j . The cosine law subsequently gives:

$$(\mathbf{X}_j - \mathbf{X}_i) \cdot (\mathbf{X}_k - \mathbf{X}_i) = \frac{1}{2} (d_{ij}^2 + d_{ik}^2 - d_{jk}^2)$$

If all measurements were perfect (i.e., noise-free), a good way to solve the location problem would be to choose some X_0 to be the origin of the coordinate system and construct the matrix \mathbf{B} accordingly, as follows:

$$\mathbf{B} = \mathbf{X}' \mathbf{X}'^T$$

where $\mathbf{X}' = \mathbf{X} - \mathbf{X}_0$.

We could then determine \mathbf{X}_0 by taking an eigen decomposition of \mathbf{B} into an orthonormal matrix of eigenvectors \mathbf{V} and a diagonal matrix of the matching eigenvalues \mathbf{U} , i.e.

$$\mathbf{B} = \mathbf{X}' \mathbf{X}'^T = \mathbf{U} \mathbf{V} \mathbf{U}^T$$

$$\mathbf{X}' = \mathbf{U} \mathbf{V}^{\frac{1}{2}}$$

In real systems however, distance measurements are obviously affected by errors (See e.g., section 3). For this reason LMDS requires to use a special point in the center of the set $\{\mathbf{X}_i\}$. This point is found by “double-centering” the squared matrix \mathbf{D}^2 . \mathbf{B} is thus given then by:

$$\mathbf{B} = \mathbf{X} \mathbf{X}^T = -\frac{1}{2} \mathbf{J} \mathbf{D}^2 \mathbf{J}$$

$$\mathbf{J} = \mathbf{I} - \frac{1}{n} \mathbf{e} \mathbf{e}^T$$

where \mathbf{e} is $1 \times n$ vector of ones. As before, the dimensionality is achieved by taking an eigen decomposition of \mathbf{B} then, removing eigenvalues and eigenvectors. This is a safe operation since \mathbf{B} is symmetric positive definite, and therefore it has n positive eigenvalues.

$$\mathbf{B} = \mathbf{X} \mathbf{X}^T = \mathbf{U} \mathbf{V} \mathbf{U}^T$$

$$\mathbf{X} = \mathbf{U} \mathbf{V}^{\frac{1}{2}}$$

Thus, the nominal LMDS provides a method for converting a complete matrix of erroneous distance measurements to a matching topology in a 2D or 3D coordinates system.

- *Proposed enhancements*

In order to improve the previous nominal LMDS technique in our specific WBAN context, we propose to follow two approaches. The first consists in using a part of the distance matrix (the most reliable components) and to reconstruct it. The second improvement introduces additional WBAN-specific constraints on the estimated distances used as inputs. This study and the related results are reported in one conference paper [MLU_ WPNC12].

SVD reconstruction:

As previously seen in section 3, due to significant shadowing effects caused by the human body, the distance matrix may present erroneous values and even in some cases, unrealistic ones. Hence the idea here is to come up with an incomplete distance matrix first, containing

only the most reliable values. The complete distance matrix, which is necessary as input to the LMDS algorithm (applied as a final step), must be reconstructed out of this incomplete version.

The reconstruction algorithm is based on [DJMPVS_06] and the property that, in a 3D coordinate system, the rank of a distance matrix cannot exceeds 5. As a consequence, a set of $10n$ judiciously chosen entries are likely sufficient to properly rebuild the distance matrix.

For the sampling task, a general and realistic model is described in [DJMPVS_06], including a connectivity disk model setting $p_{ij} \approx 1$ if $d_{ij} < R$ and $p_{ij} \approx 0$ otherwise. Here R denotes the sensor radius and $p_{ij} \in [0, 1]$ denotes the probability that node i has successfully measured its exact distance to node j . Another assumption concerning the detection probability was $p_{ij} > p_\epsilon > 0$ for all $i, j = 1 \dots n$, for some small positive constant p_ϵ . In other words, we assume that even distant far-away sensors have a very small but non-null probability of measuring the relative distance.

We thus define the incomplete matrix of estimated relative distances by its entries, as follows:

$$\hat{D}_{ij} = \begin{cases} d_{ij}^2 + \epsilon_{ij} & \text{with probability } p_{ij} \\ ? & \text{with probability } 1 - p_{ij} \end{cases}$$

The question mark in the above formalism just denotes that the entry is unknown (i.e., incomplete part of the matrix).

The reconstruction algorithm thus takes as input the previous incomplete distance matrix \hat{D} and, as a first step, we construct another matrix S with entries:

$$\hat{S}_{ij} = \begin{cases} \frac{d_{ij}^2 + \epsilon_{ij} + \gamma_{ij}(1 - p_{ij})}{p_{ij}} & \text{if } d_{ij} \text{ was detected} \\ \gamma_{ij} & \text{otherwise} \end{cases}$$

where γ_{ij} represents “the best guess” for the distance between i and j in case there is no detection over the link. In our simulations, this best guess is forced to the squared maximum connectivity radius R^2 .

The next step is the construction of another matrix $S5$, which is the best rank 5 approximation to S , recalling that D has a rank at most 5 in practical cases. The very last step is to apply LMDS algorithm with $S5$ as input.

Min-Max relative distance constraints

Another way to improve the estimation results consists in adding constraints on estimated distances. Since the sensors are supposed to be disseminated on the body, not all the distances are physically allowed. For every single estimated distance, maximum and minimum limits

are then specified and the estimation results (i.e., after applying the previous modified LMDS) are compared to these a priori constraints. If the estimated relative distance exceeds these limits, the estimator is forced back to the maximum or minimum tolerated values. For this sake, two extreme cases are proposed. In the first case, we assume having details on every link. Accordingly, the maximum and minimum distances between each pair of sensors is supposed to be known a priori over a complete walk cycle. However in the second configuration, the a priori information is more general and we just suppose one overall maximum distance constraint to be known. These two kinds of constraints allow reducing the shadowing effect introduced by the human body on the estimated distances (in terms of both errors and missing packets/measurements).

- *Performance Evaluation*

Tested scenario and simulation set-up

The first proposed scenario consists in a moving human body with a deliberately large number of on-body sensors. The real coordinates of these sensors are given by a real C3D file while the estimated coordinates are the outputs of the modified LMDS algorithm, which takes as inputs the observed peer-to-peer distances based on RSSI (Radio Signal Strength Indicator) measurements. In these preliminary simulations, we used the path loss model proposed in the IEEE 802.15.6 standard relative to body-surface communications (i.e., CM3 - Channel Model 3). Accordingly, the path loss is modeled by:

$$PL(d)[dB] = a \log_{10}(d) + b + N$$

where PL is the path loss in dB, a and b are coefficients of linear fitting, d(mm) is the distance between the Tx and the Rx, and N is a normally distributed random variable with zero mean and standard deviation σ_N , which models the shadowing effects.

In CM3, these path loss parameters take the values reported in the **Erreur ! Source du renvoi introuvable.** 4.1 under the measurements conditions detailed in [RDGO_09]:

	Hospital Room
a	19.2
b	3.38
σ_N	4.40

Table 4.1: IEEE 802.15.6 CM3 path loss parameters used for on-body RSSI simulations

In the previous model, the relative path gain represents the variation of the path loss with respect to the mean value of the standing scenario. In fact the transmitting antenna is placed on the navel while the receiving is on different positions on the body and the human subject takes different positions: standing, walking, up and down movements. Based on RSSI

measurements, the goal is to estimate, for each acquisition time frame, the location of these sensors so as to track the body's motion.

As presented before, the two first stages of LMDS algorithm give the coordinates in an arbitrary basis. Thus we assume a priori the knowledge of three sensors' locations to reestablish the real absolute coordinates system in a global system. As it will be seen in the following, one option is to accurately localize these reference points with four IR-UWB devices in the environment (hence delivering 4 RT-ToF measurements, following a joint navigation/capture approach (See e.g., section 4.2) or to assume that those reference nodes are body-strapped (e.g., fixed at know distances on a piece of clothes). However, since it does not yet fall in the scope of these preliminary investigations, we herein just assume perfect knowledge of those reference positions first, mostly for evaluation purposes (and thus, without loss of generality in terms of relative on-body positioning performances).

The LMDS algorithm was simulated using 126 frames, containing 41 points or sensors, from a real C3D file representing a walking human. For *eigen/singular value decomposition* (SVD) reconstruction, as an example, we consider a connectivity radius $R = 500\text{mm}$ and a minimum detection probability $p_\epsilon = 0.01$.

Finally, for distance constraints, we consider the two cases:

- Case 1: maximum and minimum distances is known a priori for each pair of sensors.
- Case 2: the maximum distance that cannot be exceeded on any link, which is 2 m in our simulations.

Simulation Results

Our results are presented with snapshots of the human motions, where we show the real sensors coordinates and the positions estimated with nominal LMDS or with the proposed enhanced approaches. As an example, Figure 4.1 shows the results while applying LMDS on RSSI-based estimated distances and taking into account the body shadowing. The average position error per frame is thus around 217mm (calculated over one step equivalent to 126 frames and 1000 independent noise process realizations for this step). As seen on the figure, the results are obviously not satisfactory for motion capture applications that would require very high precision.

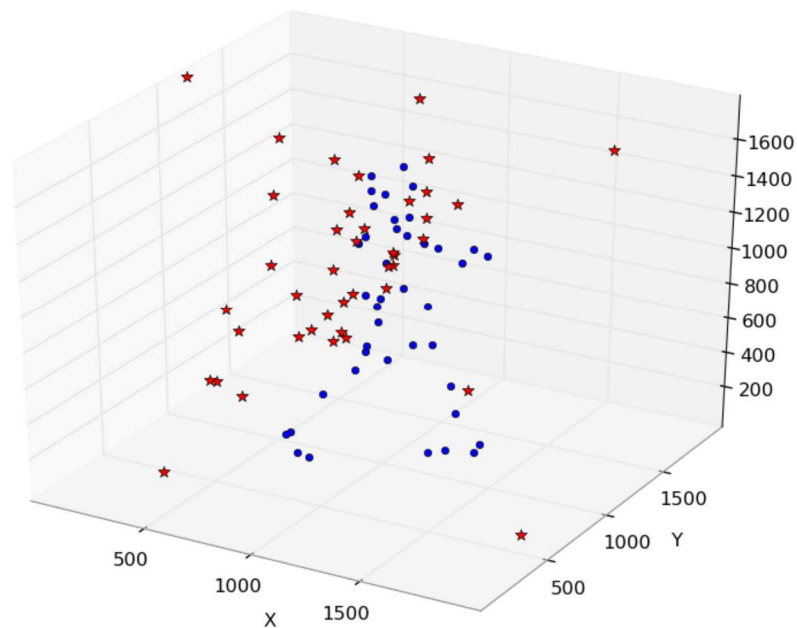


Figure 4.1: Example of real frame of on-body nodes vs. estimated frame obtained with nominal RSSI-based LMDS.

The beneficial effects of the first proposed improvement is represented on Figure 4.2 where one can generally observe a decrease of the estimation location errors, with an average error around 167mm, representing a 22% improvement that would still be insufficient to cover conventional motion capture needs. Figure 4.3 finally shows the obtained LMDS results with both SVD reconstruction and a priori distance constraints (within case 1). The latter figure then qualitatively shows significant performance gain, with an average positioning error per frame equal to 37mm, representing an improvement by 76% in comparison with conventional LMDS.

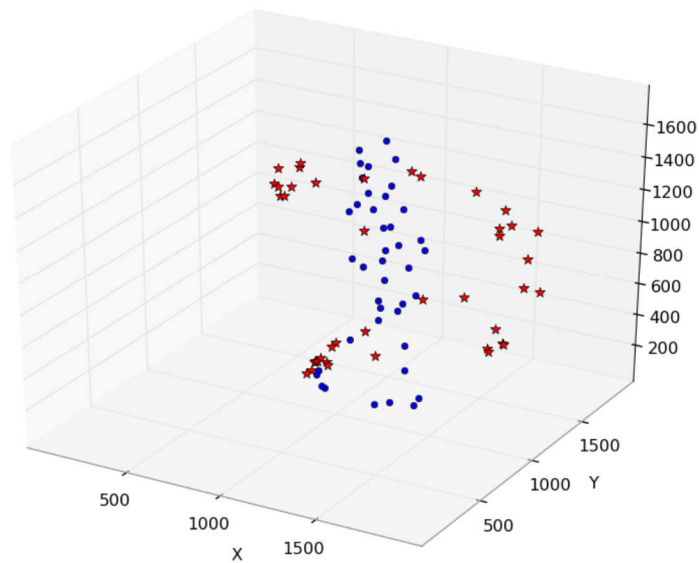


Figure 4.2: Example of real frame of on-body nodes vs. estimated frame obtained with RSSI-based LMDS and SVD reconstruction.

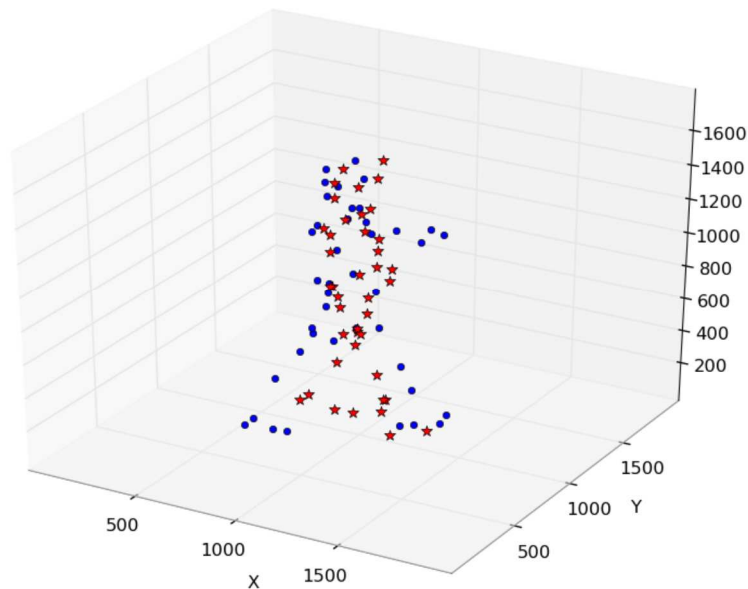


Figure 4.3 : Example of real frame of on-body nodes vs. estimated frame obtained with RSSI-based LMDS, SVD reconstruction and a priori min-max distance constraints (Case 1).

Under the same simulation conditions, we also represent on Figure 4.4 the CDF of positioning errors (over one walk cycle and over noise realizations) for different combinations of the three previous techniques. This figure shows that for conventional LMDS, errors are lower than 250mm in 80% of time, whereas for LMDS with SVD reconstruction and distance constraints, this error is reduced down to 50mm. Comparing LMDS with SVD reconstruction and LMDS

with distance constraints only, the figure also shows that over all the error regimes, the method with a priori distance constraints provides better results, because clipping significantly reduces body shadowing effect. This tends to emphasize the importance of integrating WBAN specificities in the on-body positioning problem.

Note that Figure 4.4 is obtained while considering only case 1 for setting a priori distance constraints (which are not always fully reliable). Similar results are shown on Figure 4.5 within case 2 with more limited a priori information. As shown, the improvement after setting such constraints is now less significant and even almost negligible after SVD reconstruction. This may be due to the fact that SVD reconstruction already implicitly enforces a limit on the distances. The main advantage, even if limited, is to remove unrealistic distance measurement outliers. The improvement strongly depends on the clipping strategies. However, the calibration information required in case 1 could be reasonably to obtain in specific application domains, e.g. in the medical field.

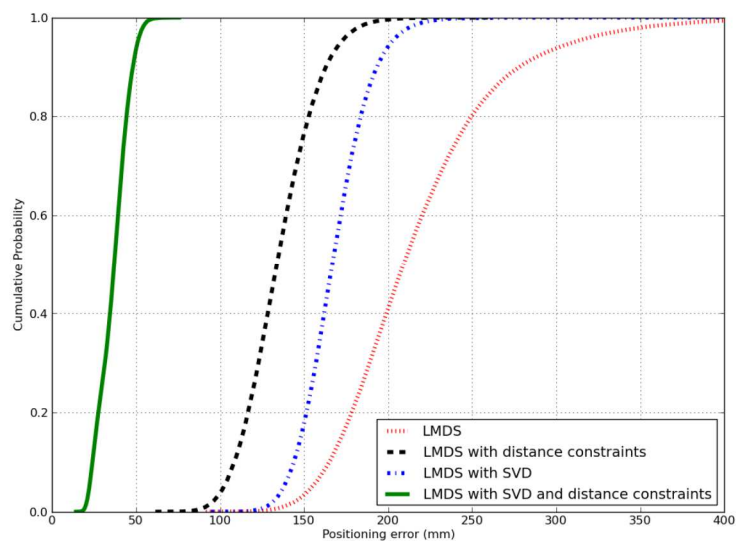


Figure 4.4: CDF of positioning error for different localization techniques (case 1 for a priori distance constraints)

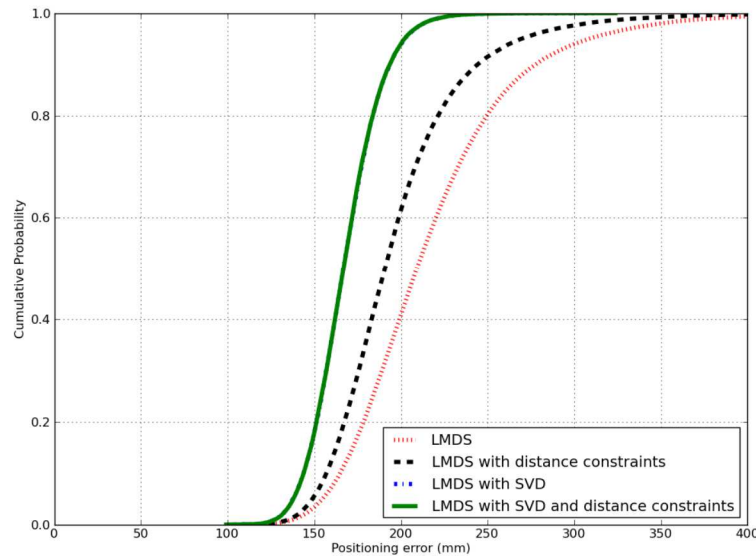


Figure 4.5: CDF of positioning error for different localization techniques (case 2 for a priori distance constraints)

Overall, the preliminary results obtained with this first centralized/synchronous LMDS technique show that WBAN-specific heuristics are clearly beneficial into the on-body positioning problem. However, i) a large of on-body nodes is still assumed number (i.e. larger than the specifications in [CORMORAN_D1.1]), ii) the positions of the reference nodes forming the local coordinates system are assumed perfectly known and iii) Only RSSI-based range measurements have been considered so far.

4.1.2 COOPERATIVE LOCALIZATION THROUGH CONSTRAINED DISTRIBUTED WEIGHTED MULTIDIMENSIONAL SCALING

We now consider coupling a *Constrained Distributed Weighted Multi-Dimensional Scaling* algorithm (CDWMDS), which asynchronously estimates the nodes' locations under geometric constraints related to fixed-length links, with new messages censoring, location updates scheduling and forced measurements symmetry. The initial motivation for adopting a decentralized approach here is to provide better immunity against the latency effects observed within classical centralized schemes under mobility, as well as better adaptability to local nodes' velocities. In centralized approaches, the time elapsed between the collection of the distance measurements and the delivery of location estimates, while the body gesture can change rapidly during the measurements collection step, tends to degrade localization performances. Motivated by the possibility to mitigate these harmful latency effects, but also to operate under partial connectivity and/or under potentially large measurement errors, we thus herein seek to estimate the nodes' positions using a distributed version of the LMDS. Another idea is to mitigate error propagation in such decentralized approaches (e.g. with respect to the fastest nodes), as well as harmful effects caused by the loss of critical packets. In line with developments carried out in T3.1 regarding *Medium Access Control* (MAC), we also

consider a beacon-aided *Time Division Multiple Access* (TDMA) scheme to suitably support both peer-to-peer ranging and decentralized positioning transactions under real-time constraints. Simulation results are provided to assess the performance of the proposed solution for various levels of connectivity and ranging quality, showing interesting gains on the average location error per node under moderate pedestrian mobility. Comparisons are finally provided with the initial centralized and synchronous LMDS algorithm described in section 4.1.1, which would require completing the matrix of measured distances under partial network connectivity.

Contrarily to the centralized synchronous LMDS case, the wireless devices placed on the body are now classified into two categories. Simple mobile nodes with unknown positions (under arbitrary deployment) must be located relatively to reference anchors nodes, which are attached onto the body at known and reproducible positions, independently of the body attitude and/or mobility (e.g. on the chest or on the back). A set of such anchors define a stable local Cartesian system LCS, which remains unchanged under body mobility. Mobile nodes are then located in the LCS, still using peer-to-peer range measurements between pairs of devices (i.e. between mobile nodes or between nodes and fixed anchors) as in the previous LMDS case. Figure 4.6 shows a typical deployment scenario, where the LCS is obviously in movement and misaligned relatively to any global coordinate system GCS. In the following, $X_i(t)$, $i = 1...m$ represent the 3D known positions of the m anchors at time t defined into the LCS, where m should be equal or larger than 3. $X_i(t)$, $i = 1...n$ represent the true 3D unknown positions of the n mobile nodes deployed on the body, at time t . Let be a range measurement available at time t between nodes i and j and let l_{ij} be a constant distance (i.e. constant over body mobility), which will be considered hereafter as a constraint.

Given the set of all available pair-wise range measurements $\{\tilde{d}_{ij}(t)\}$, now based on e.g. IR-UWB ToA estimation [GTGKMPS_05], [HDER_ACM13], based on existing constraints related to the body geometry and based on the known anchors' locations, the problem that we want to solve is still to estimate the positions of the mobile nodes into the LCS.

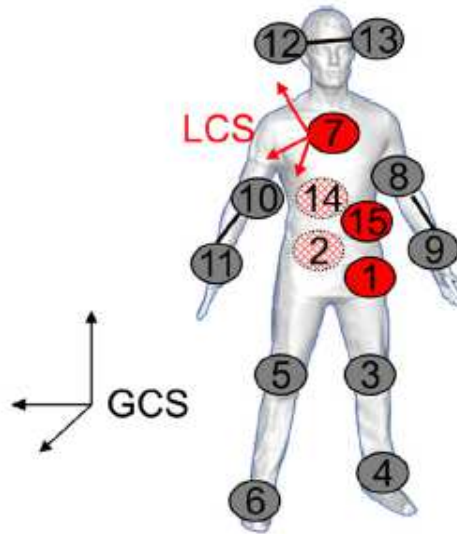


Figure 4.6: Typical deployment scenario for the relative localization of on-body wireless nodes (grey circles) with respect to a body-strapped Local Coordinate System (LCS) defined by fixed anchors (red circles), along with constant-length link constraints (black lines).

- *Basic Distributed Weighted Multidimensional Scaling Algorithm (DWMDs)*

In [HDR_ACM13], [JH_PhD_13] (and partly with section 4.1.1 herein), the applicability and the main challenges of conventional multi-dimensional scaling (LMDS) into our specific cooperative WBAN context have been pointed out and discussed.

As described in Costa et al. [CPH_06], the *Distributed Weighted Multi-Dimensional Scaling* (DWMDs) allows each node i with unknown coordinates to localize itself by minimizing a local cost function as follows:

$$\hat{X}_i(t) = \underset{X_i(t)}{\operatorname{argmin}} \left[\sum_{j=1}^n w_{ij}(t) (\delta_{ij}(t) - d_{ij}(\hat{X}(t)))^2 + \sum_{j=n+1}^{n+m} 2w_{ij}(t) (\delta_{ij}(t) - d_{ij}(\hat{X}(t)))^2 + r_i(t) \|X_i(t) - \bar{X}_i(t)\|^2 \right]$$

where $\hat{X}_i(t)$ is a vector containing the estimated 3D coordinates of node i , n and m are respectively the number of blind nodes with unknown locations (i.e. nodes must be localized) and the number of anchors placed on the body, $\hat{X}(t)$ is the matrix whose columns contain the estimated positions for all the nodes at time t , $\delta_{ij}(t)$ is a so-called observed/measured distance

between node i and j at t , $d_{ij}(\hat{X}(t))$ denotes the Euclidean distance between i and j built out of estimated coordinates, which is equal to

$$\sqrt{(\hat{X}_i(t) - \hat{X}_j(t))^T (\hat{X}_i(t) - \hat{X}_j(t))}$$

$w_{ij}(t)$ is a weight value, which reflects the connectivity and/or the accuracy of the range measurements between nodes i and j at time t , such that inaccurate measurements are down-weighted in the cost function, $\bar{X}_i(t)$ is a vector with prior information about the position occupied by node i at time t , while $r_i(t)$ quantifies the reliability of this prior information.

As described in Costa et al. [CPH_06], at each time t , the optimization problem is iteratively resolved to estimate the nodes' positions. If $\hat{X}^{(k)}(t)$ is the matrix of the estimated positions at iteration k , node i derives its current coordinates update as follows:

$$\hat{X}_i^{(k)}(t) = a_i(t)(r_i(t)\bar{X}_i(t) + \hat{X}^{(k-1)}(t)\mathbf{b}_i^{(k-1)}(t))$$

where

$$a_i(t) = \sum_{j=1}^n w_{ij}(t) + \sum_{j=n+1}^{n+m} w_{ij}(t) + r_i(t)$$

and $\mathbf{b}_i^{(k)}(t) = [b_1^{(k)}(t), \dots, b_{n+m}^{(k)}(t)]$ is a vector whose entries are given by

$$b_j(t) = w_{ij}(t) \left[1 - \frac{\delta_{ij}(t)}{d_{ij}(X^{(k)}(t))} \right] \quad j \leq n, j \neq i$$

$$b_i(t) = \sum_{j=1}^n \frac{w_{ij}(t) \delta_{ij}(t)}{d_{ij}(X^{(k)}(t))} + \sum_{j=n+1}^{n+m} \frac{w_{ij}(t) \delta_{ij}(t)}{d_{ij}(X^{(k)}(t))}$$

$$b_j(t) = 2w_{ij}(t) \left[1 - \frac{\delta_{ij}(t)}{d_{ij}(X^{(k)}(t))} \right] \quad j \geq n$$

- *Proposed Constrained Distributed Weighted Multidimensional Scaling Algorithm (CDWMDS)*

Fixed-length link constraints

In [HDR_SENS12], two first improvements have been proposed to get the nominal DWMDS more adapted into the WBAN relative localization context.

One first trivial point consists in taking the latest estimated position available for node i at time $t - 1$, as a priori information in its local current cost function, i.e. with $\bar{X}_i(t) = \hat{X}_i(t - 1)$. Note that this is not a filtering or smoothing operation but the point is just to deliver a close-enough initial guess to ease faster convergence. This choice accounts for the bounded motion amplitudes of on-body nodes under human mobility. Still relatively to the LCS, this amplitude strongly depends on the node's location itself.

The second improvement consists in using coarse a priori information about the nodes deployment to benefit from geometrical characteristics of the human body. The idea is to introduce fixed links on the body (e.g. links between hand's wrist and elbow) as constraints into the positioning problem. In particular, we use an approximated version of the true constant distances (e.g. learnt out of repeated measurements after averaging, during a preliminary calibration phase under mobility) as inputs, leading to a Constrained version of the DWMDS algorithm (CDWMDS).

Table 4.2 shows the main differences between DWMDS and CDWMDS, where $d_{ij}(t)$ is the instantaneous distance measured between nodes i and j at time t and l_{ij} is an approximated version of the fixed distance between nodes i and j , which is considered as constant over time independently of the body gesture. Accordingly, no more ranging measurements are required for these links in the steady-state localization regime. Accuracy considerations apart, CDWMDS then theoretically tends to reduce the number of exchanged packets, and hence accordingly, latency and energy consumption.

	DWMDS	CDWMDS
Fixed links	$\delta_{ij}(t) = \tilde{d}_{ij}(t)$	$\delta_{ij}(t) = l_{ij}$
Mobile links	$\delta_{ij}(t) = \tilde{d}_{ij}(t)$	$\delta_{ij}(t) = \tilde{d}_{ij}(t)$

Table 4.2: Comparison b.t.w. DWMDS and CDWMDS algorithms in terms of input range information

Another set of enhancements to the previous CDWMDS algorithm is proposed in [HDR_BOD12]. One first idea is to avoid error propagation in the retained asynchronous and decentralized approach, whereas another point consists in reducing the effects of outlier range measurements and packet losses.

Unidirectional censoring of rapid nodes' transmissions

One first goal is to mitigate error propagation while updating nodes locations. As previously mentioned, it has been illustrated in [HDR_SENS12] that the locations estimated for the most rapid nodes are affected by significantly higher errors in comparison with slower nodes. Hence, we propose to allow only the update of such fast nodes with respect to their 1-hop neighbors but no updates of these neighbors with respect to the fast nodes in return, i.e. performing some kind of unidirectional censoring. The expected gains are two-fold: keep on benefiting at rapid nodes from the reliability of their slow neighbors' estimates, but also improve the average location accuracy in the entire network by avoiding error propagation from less reliable rapid nodes. The unidirectional censoring of any rapid node j would be practically applied by forcing the weight function $w_{ij}(t)$ to be null with respect to any neighboring on-body node i (i.e. $w_{ij}(t) = 0, \forall j \leq n$ whereas $w_{ji}(t) \neq 0$).

Scheduling of location updates

The objective here is still to avoid error propagation, by forcing the algorithm to converge properly first after updating in priority the slowest and most reliable nodes. Hence, rapid nodes benefit from the consolidated reliability of their slow neighbors' estimates and error propagation is minimized. Practically, within a coordinated medium access scheme of the multiple on-body nodes as it will be seen hereafter, where all the protocol transactions shall be scheduled (i.e. for both range measurements and position updates), one can keep track of the approximated dynamic speeds on the coordinator side, based on the latest available position estimates. Hence, at each new time stamp (and hence, at each superframe), one can draw such an ordered list setting the nodes to be updated in priority. Finally, one more degree of freedom concerns the number of updates per node per localization cycle (i.e. per superframe) or equivalently, the refreshment rate, which can be also dynamically increased for the most demanding nodes.

Forced measurements symmetry

The objective here is to jointly mitigate measurement outliers and packet losses. Hence, we propose to force the distance measurements for each pair of nodes into being symmetric, as follows:

$$\delta_{ij}(t) = \delta_{ji}(t) = \frac{w_{ij}(t)\delta_{ij}(t) + w_{ji}(t)\delta_{ji}(t)}{w_{ij}(t) + w_{ji}(t)}$$

Practically, once the peer-to-peer range measurements between two nodes i and j are recovered independently in both directions (i.e. $\delta_{ij}(t)$ or $\delta_{ji}(t)$), our proposal consists in sharing the related information between each pair of nodes in order to mitigate possible packet losses (and thus missed measurements) that may occur during the ranging transactions. Moreover, if we suppose that the distance observed by node i from node j is strongly affected by measurement noise and/or bias (i.e. $\delta_{ij}(t)$) but that the distance observed by node j is less noisy, outliers are mitigated or more generally speaking, the resulting measurement variance is divided by a factor 2 after averaging.

- *Supporting Medium Access Control (MAC) for localization-enabled WBAN*

In our WBAN localization context, one key feature of the Medium Access Control (MAC) is to enable ranging between the nodes, as well as further exchanges of any kind of location-dependent information. In [MDEO_09] a first beacon-aided TDMA superframe has been presented, which was adapted for WBAN applications running on the IEEE 802.15.4 radio standard. Figure 4.7 represents the MAC superframe used in [BHMDO_10] (and directly inspired from [MDEO_09]) adapted for localization purposes. In our work, we also consider using this MAC superframe. As shown in Figure 4.7, the superframe structure is delimited by a beacon, which is transmitted periodically by the coordinator (e.g. possibly one on-body anchor here) to all the nodes in order to resynchronize all the WBAN (i.e. indicating the beginning of the superframe). The beacon fully describes the MAC superframe, specifying in particular the *Time Slots* (TSs) allocated for each transmitting node. The *Contention Access Period* (CAP) is devoted to contention based transmissions, while the *Contention Free Period* (CFP) is composed of *Guaranteed TSs* (GTSs) allocated by the coordinator. During the inactive period, the nodes may enter in a sleep mode to reduce energy consumption. The peer-to-peer range information is usually based on Round Trip - Time of Flight (RT-ToF) estimation, which relies on 2-Way Ranging (2-WR) or 3-Way Ranging (3-WR) handshake protocol transactions and unitary ToA estimates for each involved packets [MDPPO_08]. Two guaranteed TSs are involved in the simplest case of 2-WR protocol to deliver a peer-to-peer range measurement between two nodes i and j , where node i sends its request packet. Once this packet is received by node j , the latter sends its response back to the requester node i inside its own dedicated TS, after a known reply time. In turn, node i will receive this response packet and the raw estimated RT-ToF through 2-WR can be computed out of the time perceived at i between the initial request transmission and the reception of the response on the one hand, and the time perceived at j between the reception of the request and the transmission of the response. One enhancement to the 2-WR protocol consists in forcing the responder node j to transmit an additional packet inside a third TS, in order to estimate and compensate the relative clock drift between the two nodes. This packet will be received by node i , leading to a 3-WR protocol. These protocol transactions are somehow generic and shall not be restricted to on-body ranging of course (e.g., they will be also considered in the following for IR-UWB ToA-based ranging over off-body and body-to-body links).

Besides the local timers associated with unitary ToA estimates and required to compute range measurements, the payload of the ranging packets are actually exploited to carry additional information (e.g. to collect local estimated positions to the coordinator for synchronous display, to exchange pair-wise ranges in case of forced measurements symmetry, etc.).

Finally, it shall be also noted that the initial on-body protocol described above is currently optimized in CORMORAN in the frame of Task T3.1. New proposals should be made accordingly by the end of the project to provide even better support to the on-body localization functionalities.

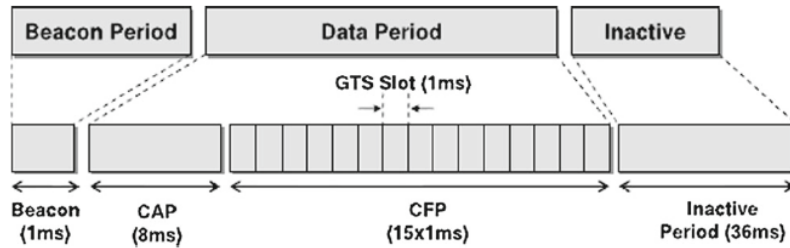


Figure 4.7: Initial beacon-aided TDMA MAC superframe format supporting localization functionalities, adapted from [MDEO_09].

- *Performance evaluation*

Tested scenario and simulation set-up

In our evaluation framework, human mobility is based on a mixed model, like in [MDEO_09]. A first macroscopic mobility *Reference Point Group Mobility* model (RPGM) accounts for the body center mobility, where the reference point as a function of time is a *Random Gauss Markov* (RGM) process [BHMDO_10]. The intra-WBAN mobility pattern is based on a biomechanical cylindrical model [P_05]. The body extremities are modeled as articulated objects, which consist of rigid cylinders connected to each other by joints. A snapshot of the resulting articulated body under pedestrian mobility is represented in Figure 4.8 at an arbitrary time stamp. The biomechanical model enables the generation of true inter-node distances, whatever the time stamp.

For each random realization, the reference body moves in a $20\text{m} \times 20\text{m} \times 4\text{m}$ 3D environment with a constant speed of 1 m/sec for a duration of 80 sec. The network deployment is similar to that presented in Figure 4.6, where 5 anchors are positioned at fixed locations relatively to the LCS and 10 blind mobile nodes with unknown positions must be positioned.

Regarding the physical radio parameters, we assume in first approximation that the received power is larger than the receiver sensitivity, enabling peer-to-peer communication links with a worst-case *Packet Error Rate* (PER) of 1 %, as specified by the IEEE 802.15.6 WPAN Task Group 6 [UMA_13]. This PER figure is applied onto 3-way ranging protocol transactions to emulate incomplete ranging (i.e. whenever 1 packet is lost out of 3). Inspired by the ToA-based IR-UWB ranging error model from section 3.1 and [HDER_ACM13], which has been specified in the IEEE 802.15.6 mandatory band centered around 4 GHz with a bandwidth of 500 MHz, ranging errors are added depending on the current LoS or NLoS channel configuration at time stamp t , as follows:

$$\begin{aligned} \tilde{d}_{ij}(t) &= d_{ij}(t) + n_{ij}(t) && \text{if } LOS \\ \tilde{d}_{ij}(t) &= d_{ij}(t) + n_{ij}(t) + b_{ij}(t) && \text{if } NLOS \end{aligned}$$

where $\tilde{d}_{ij}(t)$ and $d_{ij}(t)$ are respectively the measured and the real distance between nodes i and j at time t , $n_{ij}(t)$ is a centered Gaussian random variable with a standard deviation σ , and $b_{ij}(t)$ is a bias term due to the absence of direct path when estimating ToA.

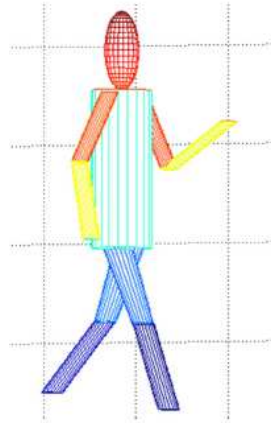


Figure 4.8: Biomechanical mobility model based on a piece-wise cylindrical representation, used in the generation of realistic inter-node distance measurements under body mobility.

Simplifying the model from section 3.1, our first simulations are carried out using a synthetic and constant σ equal to 10 cm, independently of the Signal to Noise Ratio $\text{SNR}(t)$, but still in the range of the values observed out of real measurements in section 3.1. The random positive bias $b_{ij}(t)$ is added only into NLoS conditions and follows a uniform distribution in the interval $[0, 10]$ cm. Moreover, this bias is assumed constant over one walk cycle in first approximation (i.e., $b_{ij}(t) = b_{ij}, \forall t$), which is also in compliance with first empirical observations from section 3.1 with dynamic links over NLoS portions (i.e. with reproducible bias from one walk cycle to the next).

Concerning the setting of the CDWMDS algorithm, three fixed-link constraints are imposed, as materialized with black lines in Figure 4.6. We also assume that the weight function $w_{ij}(t)$ is equal to 1 in connectivity conditions and 0 when the nodes i and j are disconnected, regardless to neighbor's information reliability (i.e. with no soft weighting under connectivity). The variable $r_i(t)$ associated with the prior estimated position of the current mobile node is taken equal to 1 like in [CPH_06] for simplification. As for the LMDS algorithm, a complete matrix is required with all the distances between all the pairs of nodes. Thus, inspired from the coarse geometric constraints used in section 4.1.1 and [MLU_WPNC12], which rely for each link on the prior knowledge of minimal and maximal feasible distances under radio connectivity. We then substitute the missed distances $\delta_{ij}(t)$ by random variables, which follow a uniform distribution in the interval $[\min_t d_{ij}(t), \max_t d_{ij}(t)]$. Localization is investigated for both CDWMDS and LMDS algorithms, considering two approaches. The first one consists in updating the nodes positions with a systematic refreshment rate of 30 ms, whereas the latency

introduced by the exchanged packets is not taken into account. However, in a second and more realistic approach, we consider a TDMA MAC superframe similar to that presented in Figure 4.7, where an *Aggregate-and-Broadcast* (A-B) procedure [MDPPO_08] is applied to ranging packets. Accordingly, under full connectivity, $3n + 2m$ transmission slots would be required to guarantee ranging transactions between any pair of nodes, instead of $2n(n + m - 1)$ otherwise. Such A-B procedures enable to share time resource in such a way that each node initiates specific ranging transactions with all the other nodes, and each transmitted packet can play different roles (i.e. either a request, or a response, or even a drift correction packet, depending on the receiving neighbor status and current step in the 3-Way procedure).

Finally, additional simulations have been carried out in order to assess localization performance as a function of the PER and standard deviation σ of intra-BAN ranging errors.

Localization performance

After running simulations of the walk cycle with 100 independent realizations of the ranging errors based on the ToA estimation and PER, localization performance is assessed in terms of the average *Root Mean Squared Error* (RMSE) per node or for all nodes. Figure 4.9 shows the average RMSE (m) for each blind node placed on the body when applying no scheduling (i.e. random) of the locations' updates. Blue bars then represent the localization performance of CDWMDS, when each measurement constraint is calculated as the mean of the measured distances in an observation window of 9 sec. Red bars show the average RMSE per node in CDWMDS using the unidirectional censoring relatively to the fastest nodes (i.e. 4 and 6). As shown in this figure, the unidirectional censoring may be efficient to improve the localization performance, decreasing the average RMSE per node from 23.3 cm down to 19.7 cm, what represents an improvement of 15.4 %. The effects of introducing scheduling in the sequence of location updates are also illustrated on Figure 4.10. Blue bars represent the localization performance of CDWMDS using our first enhancement but random scheduling for the update of nodes' locations, whereas red bars account for situations when the slowest nodes are updated in priority and the fast nodes are updated later on (i.e. 4 and 6). The average RMSE (m) per node then decreases from 19.7 cm down to 17.5 cm, representing an improvement by 11.1 %. Moreover the gain is mainly observed for the most poorly positioned nodes. Note that with location updates scheduling, the refreshment rate could be anyway adjusted depending on the local mobile speed in order to favor the most demanding nodes. Figure 4.11 shows the impact of forcing measurements Symmetry, while the blue bars represent the average RMSE per node using the CDWMDS algorithm with the two enhancements, whereas red bars show the localization performance when the distance measurements between nodes are forced to be symmetric. The average RMSE (m) per node decreases from 17.5 cm down to 15.5 cm, representing an improvement of 11.4 %. A comparison between LMDS and CDWMDS, with and without MAC superframe, is also provided on Figure 4.12 and Figure 4.13. Figure 4.12 shows the variation of the average RMSE (over all the nodes) as a function of the PER. Blue, red and green curves represent respectively the localization performance of CDWMDS, CDWMDS under forced measurements symmetry and LMDS algorithms, while the dashed curves represent the corresponding RMSE with a realistic MAC superframe. As it can be seen,

for each tested PER value, CDWMDS outperforms LMDS, with and without superframe. Moreover, this figure shows the harmful effects of the latency induced by real MAC transactions, and in particular between the collection of measurements and the positioning step. The effect is all the more noticeable with centralized approaches like within MDS. In addition, it appears that forcing measurements symmetry is indeed an efficient way to mitigate packet losses, outliers or more simply high noise. Finally, localization performance is slowly degraded at high PER, most likely due to the jointly cooperative and decentralized nature of the proposed algorithm. Figure 4.13 shows the variation of the average RMSE for all the nodes as a function of the standard deviation of on-body ranging errors. As expected, the performance is rapidly and rather strongly degraded under larger and larger measurement errors. At high noise standard deviation (e.g. larger than 20 cm), we also observe that the latency effects introduced by the use of a realistic MAC superframe are minimized, experiencing approximately similar performances (i.e. between dotted and their corresponding continuous curves). The previous observation indicates that measurement errors are by far dominating in this case in comparison with latency effects, which could hence be neglected.

In CORMORAN, in the frame of T4, the previous algorithm shall be used for the evaluation and demonstration of on-body relative positioning based on real IR-UWB devices.

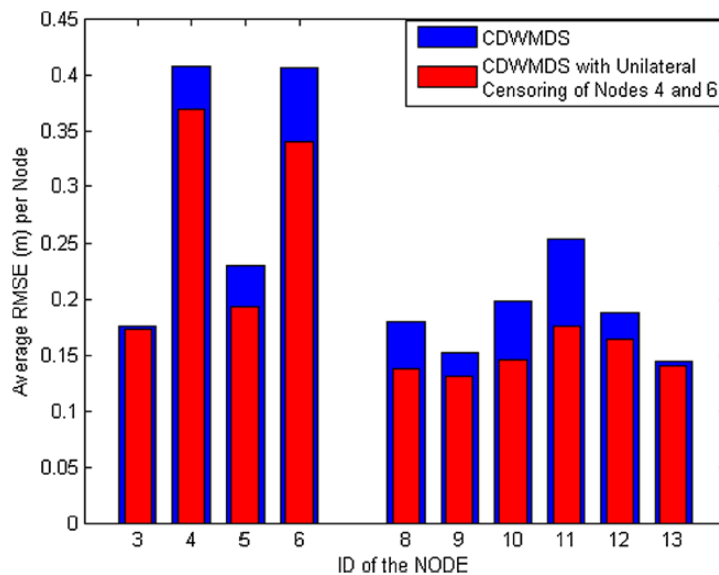


Figure 4.9: Average RMSE (m) per node with and without updates scheduling for $\sigma = 10$ cm and a refreshment rate of 30 ms.

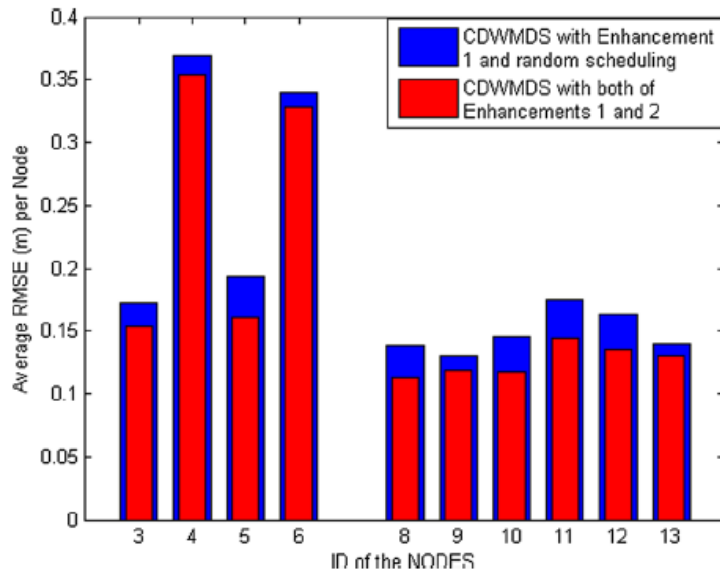


Figure 4.10: Average RMSE (m) per node with and without updates scheduling for $\sigma = 10$ cm and a refreshment rate of 30 ms.

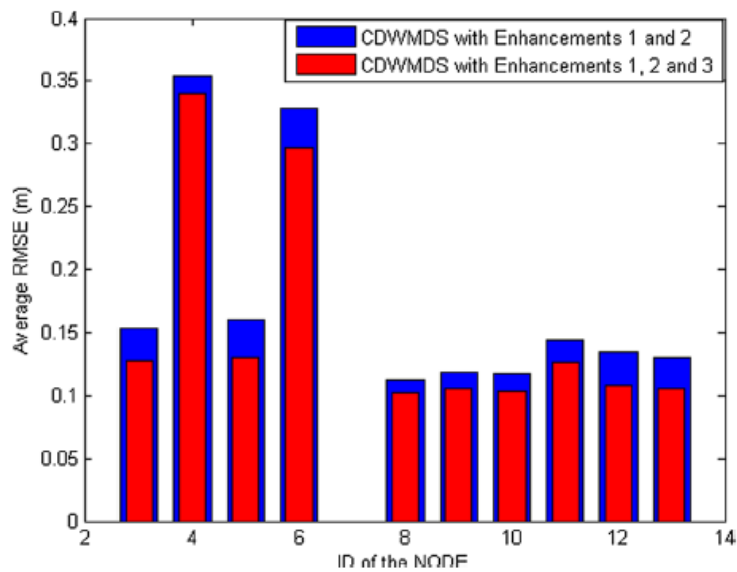


Figure 4.11: Average RMSE (m) per node with and without Forced Measurements Symmetry, with $\sigma = 10$ cm and a refreshment rate of 30 ms.

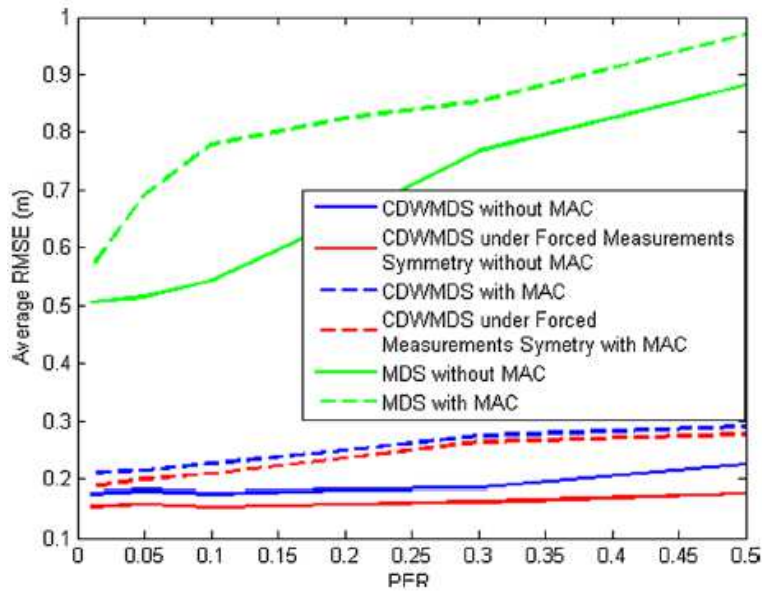


Figure 4.12: Average RMSE (m) over all the nodes in the WBAN as a function of PER, with $\sigma = 10$ cm.

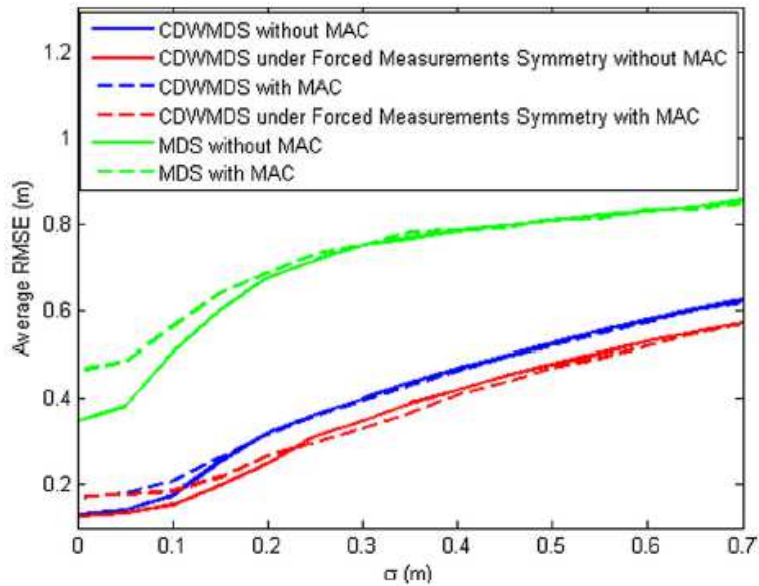


Figure 4.13: Average RMSE (m) for all the nodes in the WBAN as a function of the standard deviation of the ranging errors, with PER = 0.01.

4.2. LOCATING ON-BODY NODES IN A GLOBAL COORDINATES SYSTEM

4.2.1 2-STEP ALGORITHM WITH WITH DISTANCE APPROXIMATION OVER NEIGHBORHOOD GRAPH

In this section, we now evaluate and compare different solutions to jointly fulfil indoor navigation and motion detection/capture needs over large-scale trajectories in the context of heterogeneous WBANs. On-body devices must be localized at the building scale by combining peer-to-peer range measurements over intra-WBAN links and further measurements with respect to external anchors forming the building infrastructure. More particularly, we consider using on-body wireless links in a mesh intra-WBAN topology, as well as off-body wireless links with respect to external elements of infrastructure, set as fixed anchors. Multi-standard wireless on-body nodes are thus required, being compliant with e.g., IR-UWB IEEE 802.15.6 for intra-WBAN communications and IR-UWB IEEE 802.15.4a or IEEE 802.15.4 over larger-range off-body links. The idea is that both on-body and off-body localization procedures could mutually benefit from each other, while preserving the finest precision of relative localization over large-scale trajectories, contrarily to the first cooperative localization attempt in [BHMDO_10], where the precision of relative localization at the body scale was degraded by the introduction of off-body links. IR-UWB and a 2.4 GHz NB technologies are assumed to provide respectively *Time (Difference) Of Arrival* (T(D)OA) estimates and RSSI. Different options and scenarios are thus compared in terms of location-dependent radio metrics, synchronization constraints and transmission ranges. In a first 2-step scheme, the positions of on-body nodes are preliminarily estimated in a body-strapped local coordinates system LCS before being expressed into an absolute global coordinates system GCS after a set of transformations. The second option considers localizing directly the nodes into the GCS using all the available measurements. Finally, we also propose a method to approximate measurements over obstructed/erroneous/missing links, by computing the shortest distance according to local graph neighborhood. On this occasion, we take advantage of the presence of multiple on-body nodes to mitigate body obstructions with respect to external anchors through distance approximations.

We first assume a set of fixed anchor nodes placed at known positions in the indoor environment and forming the building infrastructure. These nodes will be also depicted as infrastructure anchors in the following. A second set comprises wireless devices placed on the pedestrian body. Just like in section 4.1.2, these devices are classified into two categories, namely simple on-body mobile nodes with unknown positions under arbitrary deployment and reference on-body anchors. The latter are attached onto the body at known and reproducible positions independently of the body attitude and/or mobility (e.g. on the chest or on the back). A set of such on-body anchors then define a stable Cartesian LCS, which remains unchanged and time-invariant under body mobility.

Figure 4.14 shows a typical deployment scenario, where the LCS is obviously in movement and misaligned relatively to an external GCS. In the following, $\{X_i^{ac}\}_{i=1..N_a}$ represents the set of the absolute 3D known positions of the N_a fixed infrastructure anchors expressed in the GCS,

where N_a should be equal or larger than 4. $\{X_i^a(t)\}_{i=1..n}$ and $\{X_i^r(t)\}_{i=1..n}$ represent respectively the absolute and relative 3D unknown positions of the n mobile nodes deployed on the body at time t , as respectively expressed in the GCS and LCS. Similarly, $\{X_i^a(t)\}_{i=n+1..n+m}$ and $\{X_i^r\}_{i=n+1..n+m}$ represent respectively the absolute 3D unknown positions of the m on-body anchors at time t and their corresponding relative known positions (supposed to be time-invariant), where m should be equal or larger than 4. Now let $\tilde{d}_{ij}(t)$ be one range or pseudo-range measurement available at time t between one on-body node i and a connected node j , j being one on-body node, one on-body anchor or one infrastructure anchor, and let l_{ij} be a constant distance (i.e. time-invariant over body mobility whatever the coordinates system), which will be considered hereafter as a constraint like in section 4.1.2 and [HDR_SENS12].

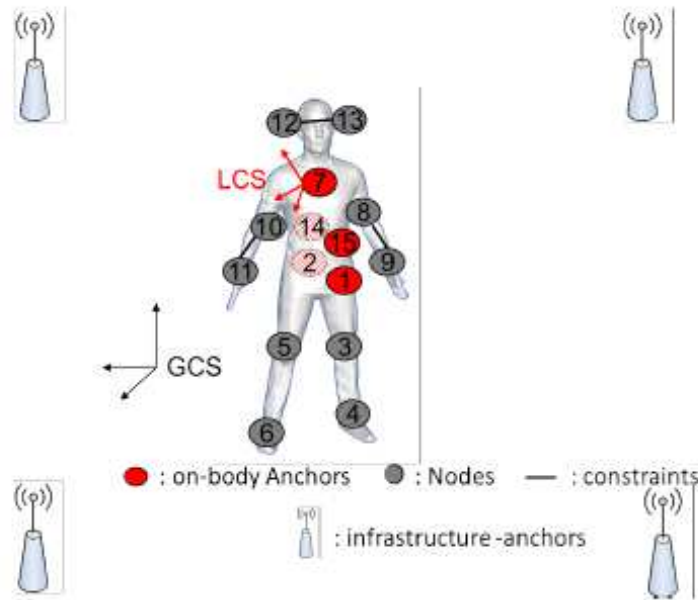


Figure 4.14 : Typical heterogeneous deployment scenario for the absolute localization of on-body wireless nodes (i.e., similarly to Figure 4.6 but now including off-body links w.r.t. external anchors).

Given the set $\{\tilde{d}_{ij}(t)\}$ of all the available measurements at time t , e.g. based on IR-UWB ToA estimation between cooperative on-body devices or between on-body nodes and infrastructure anchors, on the known locations of on-body anchors and infrastructure anchors, the problem that we want to solve consists in estimating the absolute positions of the on-body nodes in the GCS.

- Proposed 2-Step LSMIC approach

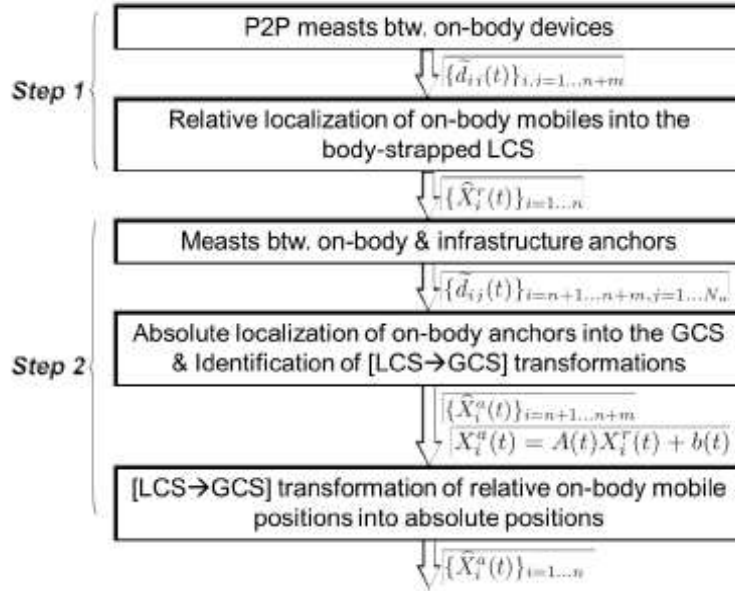


Figure 4.15 : 2-step LSMIC algorithm.

- 1-st Step: The idea is to start the LSMIC procedure by localizing the on-body nodes relatively to the LCS, using cooperative peer-to-peer range measurements between pairs of devices. We propose to apply the CDWMDS algorithm described in section 4.1.2, which is intended for relative on-body localization in the WBAN context. According to the new introduced formalism, each node localizes itself by minimizing a local cost function that depends on its neighborhood information, as follows:

$$\begin{aligned}
 \hat{X}_i^r(t) = & \operatorname{argmin}_{X_i^r(t)} \left[\sum_{j=1, j \neq i}^n w_{ij}(t) (\delta_{ij}(t) - \hat{d}_{ij}(X_i^r(t), \hat{X}_j^r(t)))^2 \right. \\
 & + \sum_{j=n+1}^{n+m} 2w_{ij}(t) (\delta_{ij}(t) - \hat{d}_{ij}(X_i^r(t), \hat{X}_j^r(t)))^2 \\
 & \left. + r_i(t) \|X_i^r(t) - \bar{X}_i^r(t)\|^2 \right]
 \end{aligned}$$

where $\hat{X}_i^r(t)$ contains the estimated 3D coordinates of node i in LCS available at time t , $\delta_{ij}(t)$ is a so-called observed distance between node i and j at t , $\hat{d}_{ij}(X_i^r(t), \hat{X}_j^r(t))$ denotes the Euclidean distance between nodes i and j , which is built out of estimated coordinates in LCS, $w_{ij}(t)$ is a weight value, which reflects the connectivity and the accuracy of the range measurements between nodes i and j at time t , $\bar{X}_i^r(t)$ is a vector

with prior information about the position occupied by node i at time t (here, $\bar{X}_i^r(t) = \hat{X}_i^r(t-1)$ like in section 4.1.2), while $r_i(t)$ quantifies the reliability of this prior information.

We also consider introducing fixed on-body links (e.g. links between hand's wrist and elbow) as constraints into the positioning problem like in section 4.1.2.

- 2) 2-nd Step: The second stage consists in converting the relative locations defined into the LCS to absolute locations into the GCS. This transformation of LCS includes a rotation and a translation. Whereas on-body anchors are time-invariant in the LCS under mobility, it is preferable to rely on those nodes to transform the LCS. In 3D environments, the absolute locations of at least 4 on-body anchors are needed to find the absolute locations of the other mobile nodes. Hence, we determine the absolute localization of the on-body anchors into the GCS first. Based on both known on-body ranges and range measurements with respect to external anchors, on-body anchors are localized through non-linear least squares optimization, by minimizing a new local cost function as follows:

$$\hat{X}_i^a(t) = \underset{X_i^a(t)}{\operatorname{argmin}} \left[\sum_{j=n+1, j \neq i}^{n+m} w_{ij}(t) (d_{ij}(t) - \hat{d}_{ij}(X_i^a(t), \hat{X}_j^a(t)))^2 + \sum_{k=1}^{N_a} w_{ik}(t) (\delta_{ik}(t) - \hat{d}_{ik}(X_i^a(t), X_k^{ae}))^2 \right]$$

where $\hat{X}_i^a(t)$ is the vector of the estimated 3D coordinates of on-body anchor i into the GCS at time t , N_a is the number of infrastructure anchors and $\delta_k(t)$ is the observed distance between on-body anchor i and infrastructure anchor k .

Getting back to our initial aim of localizing on-body nodes into the GCS, the absolute coordinates can be obtained out of the relative coordinates into the LCS after a few transformations (i.e. rotation and a translation), which can be represented as follows:

$$X_i^a(t) = A(t)X_i^r(t) + b(t)$$

The goal now is to estimate the rotation matrix $A(t)$ and the translation component $b(t)$ out of noisy observations, by minimizing the difference in the least squares sense between the absolute locations of on-body anchors and the corresponding versions, which are obtained through the transformation of estimated relative positions. For a given on-body anchor l , we set $\Delta X^r(t) = [\Delta X_{n+1}^r(t), \dots, \Delta X_{l-1}^r(t), \Delta X_{l+1}^r(t), \dots, \Delta X_{n+m}^r(t)]$ and $\Delta X^a(t) = [\Delta X_{n+1}^a(t), \dots, \Delta X_{l-1}^a(t), \Delta X_{l+1}^a(t), \dots, \Delta X_{n+m}^a(t)]$ where $\Delta X_i^r(t) = X_i^r(t) - X_i^r(t)$

and $\Delta X_i^a(t) = X_i^a(t) - X_l^a(t)$ for $l \neq i$. The alignment problem can therefore be formulated as a least-squares optimization problem, as follows:

$$\hat{A}(t) = \underset{A(t)}{\operatorname{argmin}} \sum_{i=n+1, i \neq k}^{n+m} \|A(t)\Delta X_i^r(t) - \Delta X_i^a(t)\|^2$$

The analytical solution of this linear least-squares problem is given by $\hat{A}(t) = \Delta X^a(t)(\Delta X^r(t))^T (\Delta X^r(t)(\Delta X^r(t))^T)^{-1}$. Finally, the absolute locations of all the on-body mobile nodes in the GCS are derived from their corresponding relative versions in the LCS, as follows:

$$\hat{X}_i^a(t) = \hat{A}(t)(\hat{X}_i^r(t) - \hat{X}_l^r(t)) + \hat{X}_l^a(t)$$

- *Direct single-Step LSIMC approach*

The idea here is to compute directly the positions of on-body mobile nodes in the GCS, by combining simultaneously all the available measurements, which can be performed between on-body devices or with respect to infrastructure anchors. Accordingly, the cost function to be minimized by each on-body device i is rather similar to previously but now incorporates also cooperative distance measurements between on-body devices, as follows:

$$\begin{aligned} \hat{X}_i^a(t) = \underset{X_i^a(t)}{\operatorname{argmin}} & \left[\sum_{j=1, j \neq i}^{n+m} w_{ij}(t) (\delta_{ij}(t) - \hat{d}_{ij}(X_i^a(t), \hat{X}_j^a(t)))^2 \right. \\ & \left. + \sum_{k=1}^{N_a} w_{ik}(t) (\delta_{ik}(t) - \hat{d}_{ik}(X_i^a(t), X_k^{ac}))^2 \right] \end{aligned}$$

- *Distance reconstruction over neighborhood graphs*

A graph is usually considered as a collection of vertices (or nodes) and edges (or distances) that connect pairs of vertices. In the very WBAN localization context, we assume that the on-body devices and infrastructure anchors form such a graph. The edges, which can be weighted by the observation distances, then reflect connectivity between the different entities. So as to mitigate link obstructions, we propose to reconstruct the graph based on connectivity and measurement information, by computing the shortest distances over neighborhood graph. The idea is to start by initializing the weight of an edge between nodes i and j by the observation distance $\tilde{d}_{ij}(t)$ in case of connectivity, and by infinity otherwise. In a second step, we replace each weight (i.e. distance) by the shortest path separating the graph nodes in the local neighborhood by updating the input distance by $\tilde{d}_{ij}(t^+) = \min\left(\tilde{d}_{ij}(t^-), \sqrt{\tilde{d}_{ik}(t^-)^2 + \tilde{d}_{kj}(t^-)^2}\right)$.

We thus adopt a “triangular” approximation $\sqrt{\tilde{d}_{ik}(t^-)^2 + \tilde{d}_{kj}(t^-)^2}$ instead of e.g., a linear one $\tilde{d}_{ik}(t^-) + \tilde{d}_{kj}(t^-)$. This choice indeed appears more adaptable to the deployment of on-body devices (i.e., 2 on-body devices and an infrastructure anchor are most likely not aligned but form a triangle). Figure 4.16 shows an example for a graph having 4 nodes, with the initial graph exhibiting a disconnection between node 1 and 4 and its reconstructed version based on the shortest observed path. Our proposal, which performs distance estimation over neighborhood graph, generally leads to an important reduction of the ranging errors affecting the measured distances (e.g. outliers), and more noticeably in NLoS conditions caused by body shadowing. Moreover, missing distances under partial connectivity are approximated whenever one path has been found.

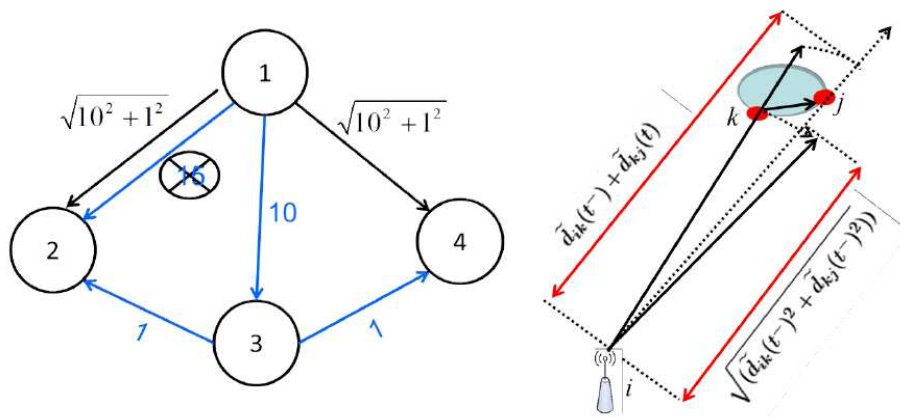


Figure 4.16 : Example of distance estimation over neighborhood graph left. The blue graph represents the initial graph based on the observation distances and connectivity information. The black graph is reconstructed based on the calculation of the shortest paths. The Right graph shows a reconstructed distance through the triangular and linear estimators.

- *Performance Evaluation*

Tested scenario and simulation set-up

Just link in section 4.1.2 and [MDEO_09], in this new evaluation framework, human mobility is still based on a mixed model. The macroscopic model accounting for the body center mobility (with a reference point following a RGM process [BHMDO_10]) is coupled with a biomechanical cylindrical-based model. Body extremities are still modeled as articulated objects, which consist of rigid cylinders connected to each other by joints.

In our scenario, for each new random realization, the reference body moves in a 20m x 20m x 4m 3D environment with a constant speed of 1m/sec for 80sec. The scene is surrounded by 8 infrastructure anchors set at the corners. The network deployment is similar to that presented on Figure 4.14, with 5 on-body anchors and 10 blind on-body nodes.

Concerning the physical radio parameters, we differentiate intra-WBAN and off-body links. We first assume IR-UWB on-body radio links, as recently promoted by the IEEE 802.15.6

standard. We also consider that the received power is larger than the receiver sensitivity, which allows peer-to-peer communications with a worst-case PER of 1%, as specified by the standard. This PER figure is applied to each single packet involved in 3-way ranging protocol transactions within the same TDMA access scheme as previously [MDEO_09], thus now emulating incomplete ranging transactions (i.e. whenever at least one packet is lost out of 3) contrarily to section 4.1.2.

Regarding on-body ToA-based IR-UWB, we consider the same conditional error model and parameters as that in section 4.1.2. As for off-body links between on-body devices and infrastructure anchors, radiolocation measurements can be delivered through IR-UWB ToA or NB RSSI estimation. In case of IR-UWB (e.g. according to the IEEE 802.15.4a standard), the conditional ToA-based ranging error model is again similar to that of section 4.1.2, but noise parameters have been adjusted according to [BHMDO_10], as reported in Table 4.3. NLoS conditions are assumed to be caused uniquely by body shadowing here (dominating effect).

Regarding NB RSSI-based ranging (e.g. according to the IEEE 802.15.4a standard in the band centered around 2.4GHz), inspired by the off-body channel model in [RE_12] and section 3.2, which has been specified in the ISM band (i.e. at 2.45 GHz), the path-loss model used in our simulations is simplified by eliminating fast fading components (i.e. considering that one would average over a sufficient number of consecutive RSSI readings per link in a real system), as follows:

$$PL(d) = PL_0 + 10n \log_{10}(d/d_0) + S$$

where $PL(d)$ is the path-loss in dB between two devices separated by a distance d , PL_0 represents the path-loss in dB at a reference distance $d_0 = 1$ m, n is the path-loss exponents and S represents the body shadowing. Simplifying further, we also suppose that S is normally distributed with zero mean and standard deviation $\sigma_S = 2$ dB.

Table 4.4 summarizes the parameters from [RE_12] and section 3.2 for WBAN planar monopole antennas and two different specific links. Note that the RSSI radiolocation metrics will be integrated only in the 2-step localization scenario, where the infrastructure anchors are just connected to on-body anchors. We have classified those links into two different sets depending on the locations of their involved on-body nodes. Generalizing the model in [RE_12], the two sets of links are thus associated with the same channel parameters as that observed for an antenna placed either on the heart or on the left hip. The estimated distance is finally extracted from RSSI readings using the *Maximum Likelihood* (ML) estimator proposed in [LAU_09].

Finally, concerning the localization algorithm setting, three fixed-length link constraints are imposed to the CDWMDS algorithm a priori like in section 4.1.2, as materialized with black lines in Figure 4.14. We also set $w_{ij}(t) = 1$ in connectivity conditions and 0 otherwise, regardless

to neighbor’s information reliability (i.e. with no soft weighting under connectivity) and $r_i(t) = 1$ for simplifications. Finally, localization updates are realized in average with a refreshment rate of 30 ms.

LOS	NLOS
$\sigma_n = 0.3$ m	$\sigma_n = 0.5$ m
$b_{ij}(t) = 0$	$b_{ij}(t) \in [1, 2]$ m

Table 4.3: TOA-based ranging error parameters over indoor off-body IR-UWB links, according to [BHMDO_10]

	LOS		NLOS	
	n	PL_0	n	PL_0
Rx heart	-2	-38.92 dB	-0.4	-62.62 dB
Rx left hip	-2	-51.94 dB	-0.1	-68.78 dB

Table 4.4: RSSI/path loss model parameters over indoor off-body NB links at 2.45GHz, according to [RE_12]

Simulation Results

Based on the previous models and settings, simulations have been carried out to illustrate and compare the LSIMC performances of both single- and 2-step localization approaches. We have also considered several options for off-body links (in the latter 2-step embodiment), integrating different radiolocation metrics, namely ToA, TDoA and RSSI. Moreover, additional simulations aim at illustrating the benefits from estimating the distances over neighborhood graph in order to mitigate obstructions and too large measurement errors. Running trials of the walk cycle with 100 independent realizations of measurement error processes, the RMSE has been characterized for each on-body mobile node. As shown on Figure 4.17, mostly due to severe obstructions and partial connectivity conditions, the performances of the standard 2-step RSSI-based and 1-step ToA-based approaches look rather poor and definitely not compliant with the requested LSIMC level of precision, even if the ToA-based option seems slightly better. However, based on IR-UWB ToA estimation over off-body links (i.e. ToA or TDoA) in the 2-step approach, rather clear gains can already be observed in comparison with the single-step approach, even though the resulting average precision would be mostly interesting to navigation application and still meaningless for LSIMC, with an average RMSE over all the on-body nodes respectively equal to 1.1 m and 1.2 m using the ToA and TDoA metrics over off-body links, hence justifying further enhancements.

On Figure 4.18, we show similar results with the additional distance estimation technique, which consists in identifying the shortest distance over neighborhood graph. The average RMSE per node is then decreased from 1.1 m down to 0.31 m, leading to a significant improvement by 72 %. On the one hand, comparable levels of precision are now achieved for absolute on-body localization at the building scale in comparison with the best performance of relative on-body localization at the body-scale in section 4.1.2 and [HDR_ACM13]. On the other hand, penalized nodes located at the body extremities, which classically suffer from

lower connectivity, poor geometric dilution of precision and higher accelerations (e.g. nodes 4, 6, 9 and 11 in our example), now seem to enjoy better robustness in comparison with other nodes. Considering relaxed deployment constraints and the claimed WBAN low consumption, these results could make this LSIMC solution a reasonable alternative to costly, power greedy and geographically restricted technologies, at least in applications requiring coarse positioning (e.g., gesture-based remote control or attitude/mobility detection).

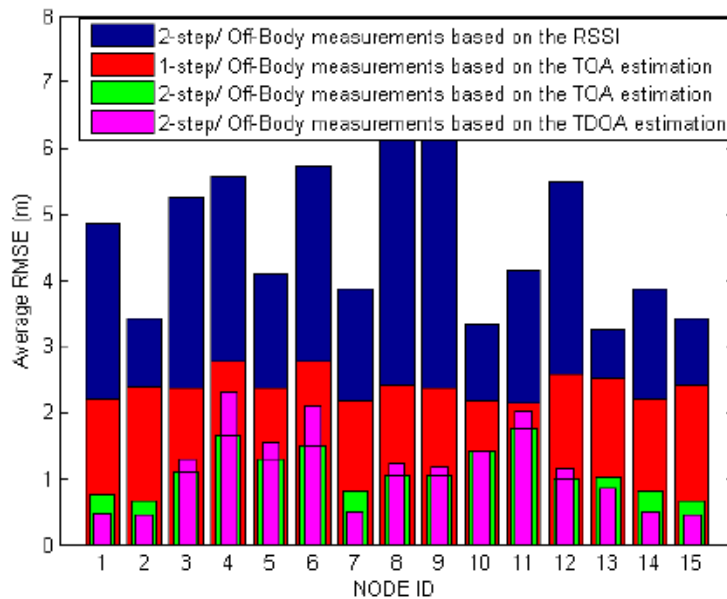


Figure 4.17 : RMSE of estimated locations per on-body node (ID) with both single and two-step LSIMC based on TOA, TDOA and RSSI metrics over off-body links.

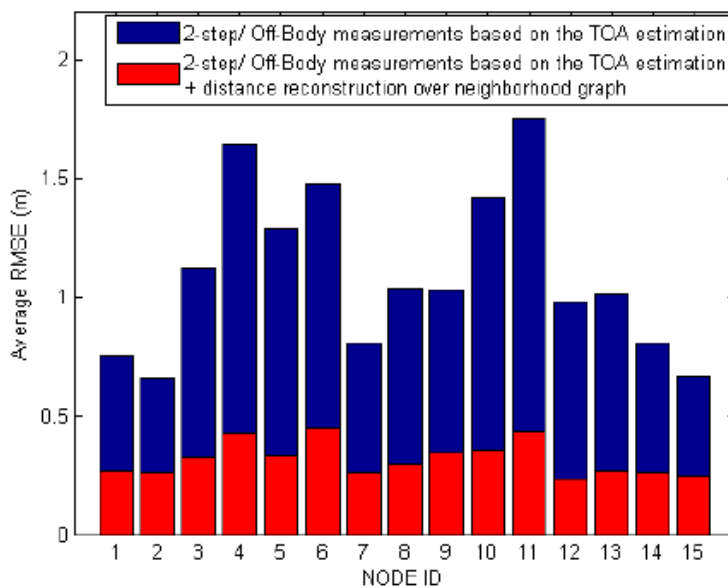


Figure 4.18 : RMSE of estimated locations per on-body node (ID) with two-step LSIMC based on TOA metrics over off-body links and distances estimation over neighborhood graph.

5. PRELIMINARY INSIGHTS ON RSSI-BASED COOPERATIVE NAVIGATION IN TYPICAL WBAN INDOOR CONTEXTS

Concerning the Inter-WBAN links, as a preliminary step of investigation in this section, we first suppose that the transmissions will use a narrowband technology rather than IEEE 802.15.6 over an UWB channel. This may be the case e.g., if the on-body nodes must be really lightweight and inexpensive and thus, if they do not include necessarily ranging-enabled sensors based on RT-ToF and multiple-way protocol transactions. Accordingly, we choose to focus on RSSI readings as input metrics, which are provided by default by communication interfaces. However, as already discussed in section 3.2, these metrics are notoriously known for providing imprecise ranging (especially at larger transmission ranges like over off-body and body-to-body), and are therefore of limited interest for localization at first sight.

We however wished first to evaluate in a more general way which level of localization was achievable in a typical indoor environment using only these metrics. To this extent, we conducted our own measurement campaign using IEEE 802.15.4 nodes and studied the variations and the correlation of the signal level indicators received by a single node from a set of other nodes.

These measurement campaigns confirmed that the log-normal shadowing approximation modeling signal attenuation is not too unrealistic. As repeatedly mentioned before, this model relates the path loss between an emitter and a receiver $PL(d)$, expressed in dB, to the distance d that separates these two nodes according to:

$$PL(d) = PL(d_0) + 10.\eta. \log_{10} \left(\frac{d}{d_0} \right) + \mathcal{N}(0, \sigma^2)$$

where $PL(d_0)$ is the path loss measured at a reference distance, which usually depends on the electronics and on the emitter and receiver design, η is the attenuation factor of the environment and $\mathcal{N}(0, \sigma^2)$ is a random variable following a normal distribution with average 0 and standard deviation σ . In most of our experiments, as the transmission power is fixed to 0 dBm, the RSSI is simply the opposite of the path loss, that is to say, $RSSI(d) = -PL(d)$.

Besides the normal distribution assumption, the relationship with distance varies according to the attenuation factor of the environment, which should be almost constant for close nodes. However, it turns out that the latter assumption is, in a general setup, not fully realistic. Indeed, experimental results show that for a given receiver, if the attenuation factor does not usually vary significantly from emitter to emitter, there are, from time to time, one or a few emitters whose measurements are not coherent with the others. We will call the sources of these incoherent measurements *aberrant* nodes in the rest of this paragraph. Aberrant nodes are inevitable in an indoor environment, due to multipath propagation essentially. The problem introduced by the presence of such aberrant nodes is that, in a parameter estimation algorithm such as maximum likelihood estimation, the η term should be different for each source, which increases the number of variables to estimate drastically.

We therefore explored the possibility to exclude one or a few sources from the estimation based on their effect on the general likelihood and replacing them by a bias, constant, term. We first examine the case of the exclusion of a single emitter from the set of emitters used by the mobile node for localization if the mobile node considers that the associated measurements do not improve localization accuracy. We select the aberrant emitter by comparing the global likelihood values obtained when each emitter is ruled out. This method requires deploying more emitters than strictly needed by trilateration (i.e. to deploy at least 4 emitters in two dimensions).

Let us denote by $RSSI_{j,L}$ the j^{th} RSSI sample measured by the mobile node on packets coming from a given emitter L . If we denote by $PL_L(d_0)$, η_L and σ_L the log-normal shadowing model specific parameters for emitter L , we can rewrite the equation above in the general case, replacing measurements coming from a given emitter O by a constant bias, β , as follows:

$$RSSI_{j,L} = \left(PL_L(d_0) + 10 \cdot \eta_L \log_{10} \left(\frac{d_L}{d_0} \right) \right) \cdot \delta_{L \neq O} + \beta \cdot \delta_{L=O} + \mathcal{N}(0, \sigma_L^2)$$

where d_L is the distance to emitter L that we try to estimate and δ is the indicator function (equal to 1 when the subscript expression is true, to 0 otherwise).

Combining all the measured values altogether, we can apply a maximum likelihood estimator on this new model to compute the likelihood expressions in the case where emitter O is considered as abnormal. If we denote by N_L the number of samples received from emitter L , the likelihood function is expressed as follows for every emitter $L \neq O$:

$$L_L(x, y) = -N_L \cdot \log \sigma_L^2 - \sum_{j=1}^{N_L} \left(\frac{RSSI_{j,L} - PL_L(d_0) - 10 \eta_L \log_{10} \left(\frac{d_L}{d_0} \right)}{\sigma_L} \right)^2$$

And for the outlier emitter, O , it becomes:

$$L_O(\beta) = -N_O \log \sigma_O^2 - \sum_{j=1}^{N_O} \left(\frac{RSSI_{j,O} - \beta}{\sigma_O} \right)^2$$

The global likelihood function, reflecting the coherence of the whole system when emitter O is excluded from the data set is then simply the sum of the previous expressions over the K emitters:

$$L_O(x, y, \beta) = \sum_{L=1; L \neq O}^K L_L(x, y) + L_O(\beta)$$

This equation can be written with each of the K emitters considered as outlier. We are then able to select which emitter will be considered as biased by computing the likelihood function for each of the $K+1$ situations. We then place ourselves in the situation that achieves the maximum likelihood, replace the selected emitter by a biased emitter if any, and compute the positions and the bias according to the following equation:

$$(x_O, y_O, \beta_O) = \arg \max_{x, y, \beta} \{L_O(x, y, \beta)\}$$

In the equation above, the $L_L(x, y)$ terms does not depend on β while the $L_O(\beta)$ term neither depends on x or on y . Therefore the likelihood equation can be solved by separating variables. The expression of the bias that maximizes $L_O(\beta)$ is straightforward:

$$\beta_L = \frac{1}{N_L} \sum_{j=1}^{N_L} RSSI_{j,L}$$

If we also consider the case in which no emitter is considered abnormal, we get $K+1$ likelihood values to compare. We then have to select the situation that yields to the best (i.e., highest) likelihood value to identify the most aberrant emitter. Experimental results show that sometimes the best likelihood corresponds to the situation in which no emitter is ruled out.

As mentioned above, there are cases in which it would be profitable to exclude more than one emitter. To study the pertinence of such an *Extended Biased Maximum Likelihood Estimation* (xB-MLE), we first examine the achieved accuracy when excluding two emitters, then three emitters in our various experimental setups. When more than one emitter is excluded, each set of measurements is replaced by a distinct bias. This allows to keep the same maximization method as above, separating variables for the optimization. For example, in the case we consider two emitters, O_1 and O_2 , for exclusion, the global likelihood function is expressed as:

$$L_O(x, y, \beta_1, \beta_2) = \sum_{L=1; L \neq O_1; L \neq O_2}^K L_L(x, y) + L_{O_1}(\beta_1) + L_{O_2}(\beta_2)$$

Nevertheless, this process does not scale. If excluding one emitter requires $K+1$ maximization operations, excluding two emitters requires a number of maximizations equal to:

$$1 + K + \binom{n}{2}$$

In order to reduce this global complexity, we derive a heuristic based on the computation of a bias gap, defined as the relative difference between the bias and the estimated average path loss. This heuristic is the corrected extension of B-MLE namely B-MLEC (*Biased Maximum Likelihood Location Estimation extension Correction*) and expressed as follows:

$$B_L = \left| \frac{\beta_L - \left(PL_L(d_0) + 10\eta_L \log_{10} \left(\frac{d_L}{d_0} \right) \right)}{PL_L(d_0) + 10\eta_L \log_{10} \left(\frac{d_L}{d_0} \right)} \right|$$

This value is computed based on the previous bias expression and hence induces a relatively low computational cost. We then compare this value with a threshold, γ , and when $B_L \geq \gamma$, emitter L is considered as abnormal. In the same way if $B_L \leq \gamma$, the emitter of index L is considered as normal. In the end, we only have one maximization operation to perform, as we can ignore all emitters that do not satisfy this condition. For the present paper scenarios we empirically chose $\gamma = 0.05$, as this value corresponds to a generally admitted rejection threshold. To confirm this threshold, we evaluated the performance of our algorithms with different threshold values (ranging from 0.004 to 0.7). Figure 5.1 represents the average localization error achieved by B-MLEC in our three testbeds and shows that error increases from a threshold value of 0.1. The best value varies with the testbed, but 0.05 seems a fair choice.

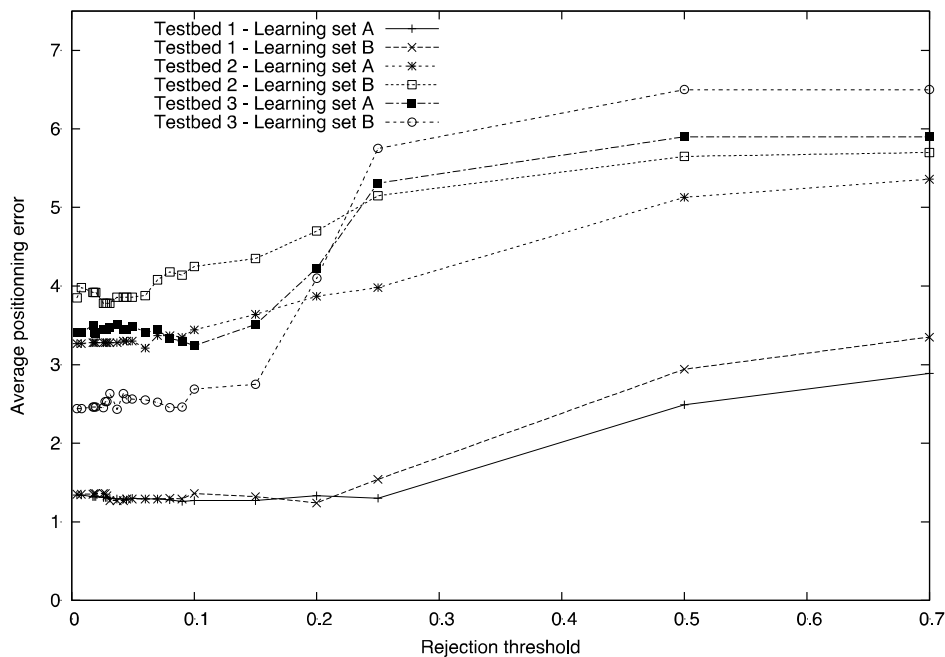


Figure 5.1: Influence of the rejection threshold on the average positioning error

These algorithms were evaluated on three different testbeds. The full results and their analysis will be available in [DCTMC_13] but are beyond the scope of this deliverable. Figure 5.2 represents an example of the median localization error of the different methods in a particular scenario.

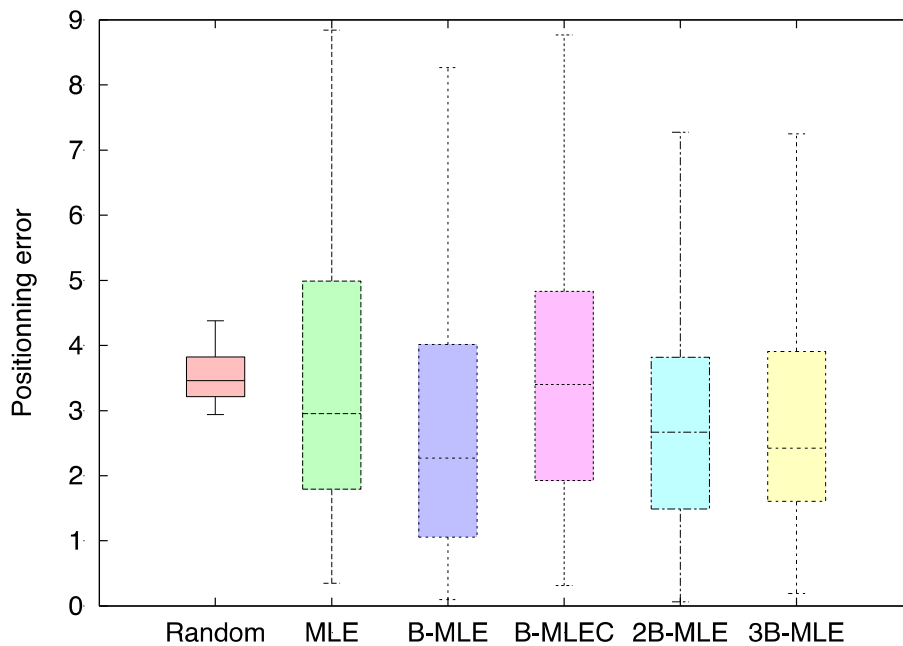


Figure 5.2: Median and standard deviation of various algorithms in a representative scenario

In this scenario, the difference between the various approaches show a slight advantage of the methods that exclude one or few emitters with respect to the classical ML estimator, or to the threshold-based approach (B-MLEC). However, that is not always the case and that is exactly the difficulty in implementing these approaches. Indeed, the algorithm that gives the best performance is not always the same and the criteria that allows selecting the appropriate approach is unclear at the time this report was written. Secondly, we can see that these methods improve the localization accuracy, but the gain is not so important so far. In the CORMORAN context, those techniques may help at least passing occasionally from an average accuracy to a good accuracy.

However in CORMORAN, the inter-WBAN scenario is slightly different from the scenario addressed in this first evaluation. Indeed, an arbitrary node belonging to a given WBAN is supposed to receive beacons from several nodes belonging to close cooperating WBANs or eventually. The other nodes located in the same WBAN will also receive the same beacons with slight variations. Correlating the difference between the measurements from the different nodes on a given body with their relative position (assumed known a priori or retrieve through on-body positioning) is thus expected to greatly improve the localization accuracy.

6. CONCLUSIONS AND PERSPECTIVES

In this deliverable, we have first characterized and discussed possible single-link ranging error representations, exploiting recent WBAN IR-UWB and 2.4GHz NB channel measurements over various kinds of cooperative links. These models rely on empirical direct modeling or theoretical predictions based on ranging performance bounds, both fed with realistic channel parameters. First of all, a dynamic on-body model has been proposed for IR-UWB ToA-based ranging in two key frequency bands and for two representative links. The drawn model, which relies on UWB channel measurements, takes into account dynamic channel obstruction configurations (i.e. LoS/NLoS) and SNR variations under body mobility. Then the related model parameters have been studied as a function of a controlled SNR within synthetic received multipath signals. On this occasion, false and missed detection phenomena have been illustrated under low SNR and NLoS conditions, as well as asymptotically ideal detection behavior under more favorable SNR and LoS conditions. The performances of first peak and strongest peak detection schemes have also been compared. We have shown that the ranging error distribution could be fairly well modeled as a centered Gaussian distribution in LoS conditions in case of systematic strongest path detection, and as a weighted mixture between uniform and Gaussian distributions in the case of first path detection. In NLoS conditions, ranging errors are also shown to follow a weighted mixture between uniform and Gaussian distributions in case of strongest path detection. Finally, a few insights have been provided for a possible extension of the previous error model to any on-body link, depending on its instantaneous LoS/NLoS and static/dynamic status. Then the model has been simplified, considering a Gaussian model, with a constant standard deviation independently of the SNR, but still in the range of the values observed over the walk cycle within the previous refined representation. Moreover, it has been assumed that the range measurements in NLoS are affected by a positive bias that follows a uniform distribution, which is also partly compliant with the previous NLoS representation. The resulting simplified model has been subsequently used to evaluate the performance of on-body localization algorithms for both relative and absolute individual MoCap purposes (See paragraphs below). Secondly, we have considered theoretical performance bounds for the standard deviation of NB RSSI-based ranging over off-body and body-to-body links, relying on realistic path loss parameters extracted from real measurements. One first conclusion, as expected, is that RSSI readings in NLoS conditions due to body shadowing are not so informative for direct conventional ranging purposes on both kinds of links (i.e., unless specific mitigation techniques are implemented), whereas LoS conditions may provide more acceptable ranging performance, but most likely at short ranges (typically below 20 m). One second remark is that off-body and body-to-body links exhibit approximately the same behaviors in terms of ranging error statistics, in first approximation, highlighting the fact that body shadowing is a dominating factor. The underlying path loss and body shadowing parameters have been partly reused in simulations while evaluating the performance of localization algorithms for joint MoCap and single-user navigation applications. These first investigation lead to the following conclusions and perspectives: i) heuristic and a priori error models could be applied to improve on-body positioning (as seen in the following herein) and ii) further investigations are still required to better exploit the obstructed links (caused by body shadowing) with respect to external nodes (i.e., either off-

body or body-to-body links). The latter point will be pursued in the frame of CORMORAN ST3.2 for the upcoming months.

Besides, in this deliverable we have also described solutions addressing the problem of WBAN-based motion capture/detection. First of all, a LMDS algorithm was improved by means of a few heuristics about maximum and minimum observable range measurements at the body scale. Then one decentralized and cooperative version has been proposed, CDWMDS algorithm, which asynchronously estimates unknown nodes' locations under geometric constraints in the form of fixed-length links. The latter has been also enhanced through scheduling and censoring to mitigate error propagation and harmful effects due to location-dependent node speed disparities. It has been shown that forced measurements symmetry could help to mitigate outliers and packet losses as well. Moreover, CDWMDS has been compared with the initial centralized synchronous LMDS algorithm in terms of localization accuracy for various PER values and for various ranging standard deviations, assuming realistic MAC protocol constraints in line with the developments currently carried out in CORMORAN ST3.1, hence illustrating the harmful effects of latency and their possible mitigation. Given the remaining observed limitations however, it appears overall that only applications requiring relatively modest on-body accuracy level could be covered by the current radiolocation technologies (e.g., gesture-based remote control, attitude/mobility detection...), instead of MoCap applications in a standard meaning. But other efforts has also been committed to couple relative on-body localization with absolute indoor positioning (i.e. with respect to fixed external anchors distributed in the environment) and/or with tracking filters, then offering enriched, "opportunistic" (out of on-body data traffic) and geographically unrestricted (through absolute positioning) capabilities.

Accordingly, we have jointly addressed the single-user navigation problem over large-scale indoor trajectories based on heterogeneous WBANs, out of preliminary on-body nodes positioning. Two approaches have thus been presented to estimate the absolute locations of on-body nodes in a global coordinates system before computing their barycenter (supposed to account for the overall body location), considering different radiolocation metrics over off-body links with respect to infrastructure anchors. One 2-step solution relies on preliminary relative localization at the body scale and applies further transformations through the absolute localization of on-body anchors. Finally, we have proposed an algorithm that estimates the shortest path between on-body and infrastructure anchors over neighborhood graph to compensate for radio obstructions and large measurement errors. Future works in CORMORAN ST3.2 will concern extensions -to a larger extent- into cooperative navigation contexts involving groups of WBANs.

Regarding the latter CGN applications, very preliminary RSSI-based measurement outliers (in turn, affecting off-body and body-to-body links) have been characterized based on indoor RSSI measurements. New methods based on several variants of global Maximum Likelihood criteria have been proposed to detect and discard aberrant measurements and replace the latter by constant biases. Those preliminary results indicate that the best selection strategy

clearly depends on the configuration of the testbed, and that the performance is improved w.r.t. classical maximum likelihood estimation in most cases, but still quite marginally. In the frame of T3.2 however, new studies regarding body-to-body and off-body cooperation in CGN applications have been recently initiated so as to better benefit from i) the natural redundancy provided by multiple on-body nodes with respect to external nodes, ii) low-complexity RSSI readings available by default over body-to-body and off-body links (but poorly informative in terms of ranging/localization so far), iii) even more advanced link/measurement selection strategy, thus opening the floor to contextual cooperation.

The last version of the deliverable (D3.5) will account for these new investigations in details. Besides, some of the previous algorithms will be evaluated by means of real field experiments in the frame of T4, based on a hardware demonstrator.

7. REFERENCES

- [CORMORAN_D1.1] C. Goursaud, B. Denis, et al., “Application Scenarios, System Requirements and Prior Models”, Deliverable D1.1 of CORMORAN, July 2012
- [HDER_ACM13] J. Hamie, B. Denis, R. D’Errico, C. Richard, “On-Body TOA-based Ranging Error Model for Motion Capture Applications within Wearable UWB Networks”, *to appear in Journal of Ambient Intelligence and Humanized Computing*, ACM/Springer
- [HDER_BOD12] J. Hamie, B. Denis, R. D’Errico, and C. Richard, “Empirical Modelling of Intra-BAN Ranging Errors Based on IR-UWB TOA Estimation”, International Conference on Body Area Networks 2012 (BodyNets’12), Oslo, Sept. 2012
- [HS_PhD_10] H. Shaban, “A novel highly accurate wireless wearable human locomotion tracking and gait analysis system via UWB radios,” PhD thesis, Virginia Polytechnic Institute and State University, 2010
- [SENB_10] H. Shaban, M. El-Nasr, and R. Buehrer, “Toward a highly accurate ambulatory system for clinical gait analysis via uwb radios,” *IEEE Trans. on Information Technology in Biomedicine*, 14(2):284{291, March 2010
- [EO_09] R. D’Errico and L. Ouvry, “Time-variant BAN Channel Characterization,” *Proc. IEEE PIMRC’09*, pp. 3000-3004, 2009
- [DK_07] B. Denis and J. Keignart, “Post-processing framework for enhanced uwb channel modeling from band-limited measurements,” *Proc. IEEE UWBST’03*, Reston, Sept. 2003, 2007
- [DRBT_07] M. Di Renzo, R. Buehrer, and J. Torres, “Ranging accuracy in uwb-based body area networks for full-body motion capture and gait analysis,” *Proc. IEEE GLOBECOM’07*, Washington DC, Nov. 2007
- [RE_12] R. Rosini and R. D’Errico, “Off-body channel modelling at 2.45 GHz for two different antennas,” *Proc. EUCAP’12*, pp. 3378-3382, 2012

- [REV_12] R. Rosini, R. d'Errico, and R. Verdone, "Body-to-body communications: a measurement-based channel model at 2.45 GHz", Proc. IEEE Personal Indoor and Mobile Radio Communications (PIMRC 2012), pp. 1763-1768, 2012
- [DJMPVS_06] P. Drineas, et al. "Distance Matrix Reconstruction from Incomplete Distance Information for Sensor Network Localization," Proc. IEEE SECON '06, Sept. 2006.
- [RDGO_09] C. Roblin, et al. "Propagation channel models for BANs: an overview," COST2100, TD(09)760, Braunschweig, Feb. 2009
- [MLU_WPNC12] M. Mhedhbi, M. Laaraiedh, and B. Uguen, "Constrained LMDS Technique for Human Motion", Workshop on Positioning, Navigation and Communication 2012 (WPNC'12), Dresde, March 2012
- [GTGKMPS_05] S. Gezici Z. Tian, G. Giannakis, H. Kobayashi, A. Molisch, H. Poor, Z. Sahinoglu, "Localization via ultra-wideband radios: a look at positioning aspects for future sensor networks," IEEE Signal Processing Mag, 22(4):70–84, 2005
- [HDR_ACM13] J. Hamie, B. Denis, C. Richard, "Decentralized Positioning Algorithm for Relative Nodes Localization in Wireless Body Area Networks", *to appear in* Journal on Mobile Networks and Applications (MONET), ACM/Springer, 2013
- [JH_PhD_13] J. Hamie, "Contributions to Cooperative Localization Techniques within Mobile Wireless Body Area Networks", PhD thesis, Université de Nice Sophia-Antipolis, Nov. 2013
- [CPH_06] A. Costa, N. Patwari, O. Hero, "Distributed weighted multidimensional scaling for node localization in sensor networks," ACM Transactions on Sensor Networks, 2(1):39–64, 2006
- [HDR_SENS12] J. Hamie, B. Denis, and C. Richard, "Constrained Decentralized Algorithm for the Relative Localization of Wearable Wireless Sensor Nodes", IEEE Sensors 2012 (IEEE SENSORS'12), Taipei, Oct. 2012
- [HDR_BOD12] J. Hamie, B. Denis, and C. Richard, "Nodes Updates Censoring and Scheduling in Constrained Decentralized Positioning for Large-Scale Motion Capture based on Wireless Body Area Networks", International Conference on Body Area Networks 2012 (BodyNets'12), Oslo, Sept. 2012
- [MDEO_09] M. Maman, F. Dehmas, R. D'Errico, L. Ouvry, "Evaluating a TDMA MAC for body area networks using a space-time dependent channel model," Proc. IEEE PIMRC'09, pp 2101–2105, Sept. 2009
- [BHMDO_10] E. Ben Hamida, M. Maman, B. Denis, L. Ouvry, "Localization performance in wireless body sensor networks with beacon enabled mac and space-time dependent channel model," Proc. IEEE PIMRC'10, pp 128–133, Sept. 2010
- [MDPPO_08] M. Maman, B. Denis, M. Pezzin, B. Piaget, L. Ouvry, "Synergetic MAC and higher layers functionalities for UWB LDR-LT wireless networks," Proc. IEEE ICUWB'08, pp 101–104, 2008
- [P_05] I. Pantazis, "Tracking human walking using MARG sensors," Technical report, DTIC Document, 2005

[UMA_13] S. Ullah, M. Mohaisen, M. Alnuem, “A review of IEEE 802.15.6 MAC, PHY, and security specifications,” International Journal of Distributed Sensor Networks, 2013

[LAU_09] M. Laaraiedh, S. Avrillon, B. Uguen, “Enhancing Positioning Accuracy through Direct Position Estimators Based on Hybrid RSS Data Fusion,” Proc. IEEE VTC-Spring’09, pp.1-5, April 2009

[HDR_WPNC13] J. Hamie, B. Denis, C. Richard, “Joint Motion Capture and Navigation in Heterogeneous Body Area Networks with Distance Estimation Over Neighbourhood Graph”, Proc. WPNC’13, Dresden, March 2013

[DCTMC_13] N.A. Dieng et al. “No-calibration localization for indoor wireless sensor networks”, Int. J. Ad Hoc and Ubiquitous Computing, *to appear* in International Journal of Ad Hoc and Ubiquitous Computing.